THE 1,3-DIPOLAR CYCLOADDITIONS OF OZONE ON THE CAP OF TWO SERIES OF [5,5] ARMCHAIR AND [9,0] ZIGZAG SINGLE-WALLED CARBON NANOTUBES CAPPED WITH FULLERENE HEMISPHERES

INTRODUCTION

Iijima *et al*., (1991) discovered carbon nanotubes with outer diameters of 4–30 nm and a length of up to 1 μm (Figure 1). These tubes consisted of two or more seamless graphene cylinders concentrically arranged with the innermost tubes, he noted, having diameters as small as 2.2 nm. Electron diffraction analysis showed that the crystal axis of the graphene sheets in some of the tubes had a helical arrangement relative to the tube axis. He called these tubes multi-walled carbon nanotubes (MWNT) because the tube diameters belonged to the nanometer order. The unique properties of these structures promised unimaginable applicability and thus attracted a great deal of interest that continues to this day. For example, super-high-quality MWNTs have recently been produced by carbon evaporation using the high-frequency plasma (Koshio *et al*., 2002). These nanotubes have a purity of over 95%, a structural uniformity with an inside diameter of 0.4 nm and an outside diameter of about 5 nm, as well as a length of the micrometer order. These super-high-quality MWNTs are thus close to the ultimate in MWNTs.

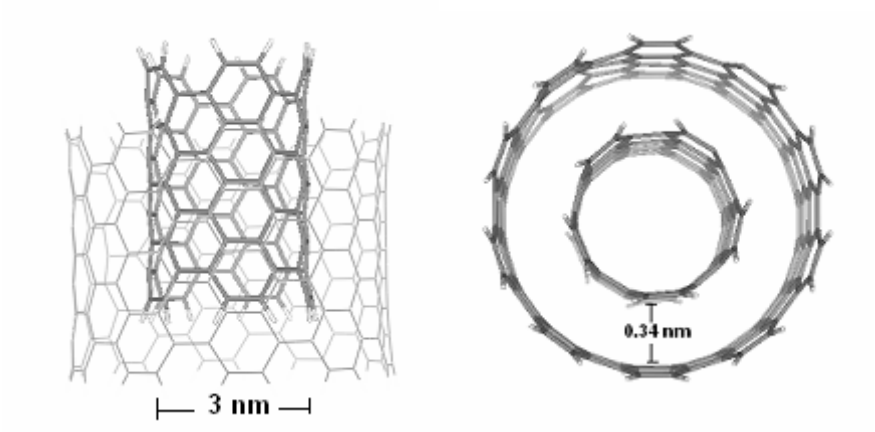

Figure 1 Multi-walled carbon nanotubes discovered in 1991.

Single-walled carbon nanotubes (SWNTs), which are seamless cylinders each made of a single graphene sheet (Figure 2), were first reported in 1993 (Bethune *et al*., 1993; Iijima *et al*., 1993). Their diameters range from 0.4 to 2–3 nm and their length is usually of the micrometer order. SWNTs usually come together to form bundles in which the SWNTs are hexagonally arranged to form a crystal-like structure (Wildoer *et al.*, 1998).

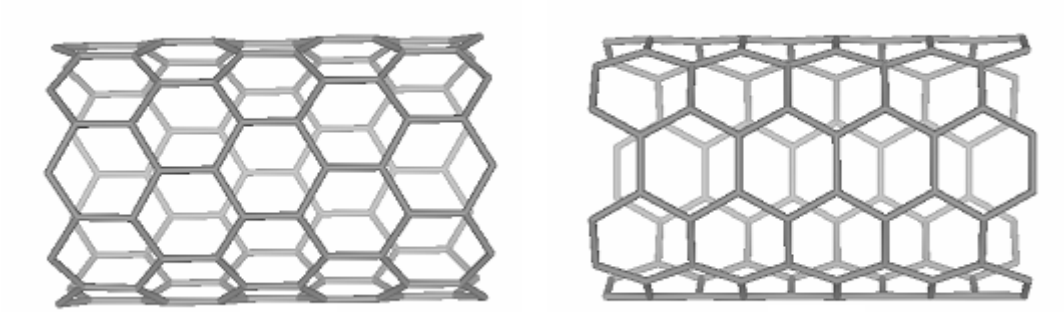

Figure 2 Side views of various nanotubes. (a) Zigzag [9,0] nanotube. (b) Armchair [5,5] nanotube. (c) Chiral [9,1] nanotube. The numbers in parentheses are the chiral indices.

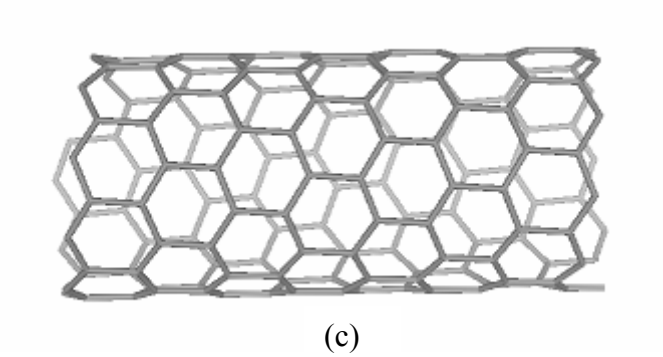

(c)

Figure 2 (Cont'd)

The electronic properties of SWNTs were found to depend on their atomic structures, which are described by their chiral angle and diameter, which are specified by the lattice indices [n,m] (Saito *et al.,* 1992; Wildoer *et al.,* 1998). Atomically resolved scanning tunneling microscope (STM) images have subsequently been used to experimentally probe the structures of SWNTs and are also used to interpret these lattice indices (Odom *et al.,* 1998; Venerma *et al.,* 2000).

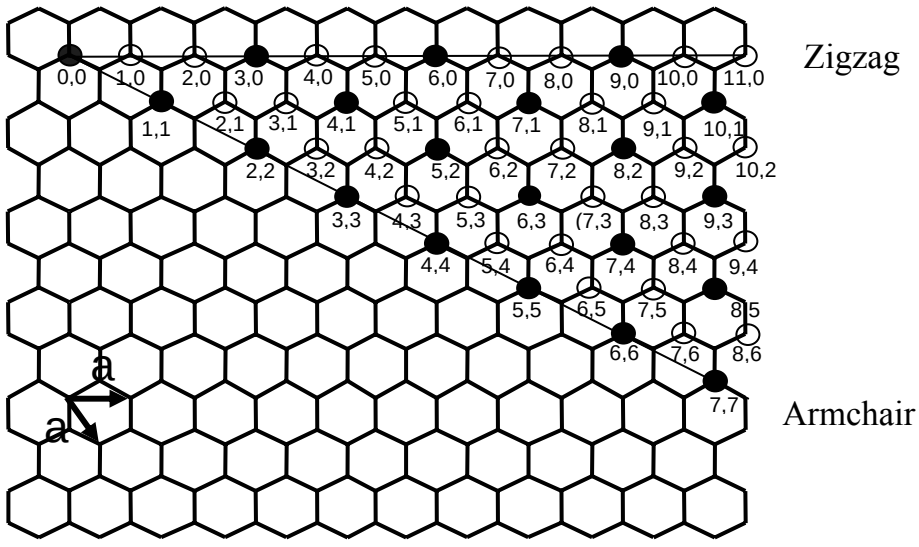

Figure 3 Flat hexagon lattices of a graphene sheet.

Figure 3 shows the origin of these indices on the flat hexagonal lattice of a graphene sheet. The structure of a SWNT can be thought of as this graphene sheet rolled into a pipe or tube. A chiral vector $\mathbf{C}_h$ in an unrolled graphene sheet is defined as $n\mathbf{a}_1 + m\mathbf{a}_2$, where n and m are integers ($0 \leq |m| \leq n$), $\mathbf{a}_1$ and $\mathbf{a}_2$ are real space unit vectors of a hexagonal lattice as shown in Figure 3. The structure of a SWNT can be represented by $\mathbf{C}_h$, which corresponds to the section of the nanotube perpendicular to the nanotube axis. Therefore, $\mathbf{C}_h$ = [n,m] defines the diameter and chiral angle of a SWNT. The chiral angle is defined to be the angle between $\mathbf{C}_h$ and the unit vector $\mathbf{a}_1$. According to the chiral angles and chiral vectors, SWNTs are classified as zigzag (Figure 2a), armchair (Figure 2b), and chiral (Figure 2c) types. The chiral angle and $\mathbf{C}_h$ of zigzag nanotubes is 0º and [n,0]. The chiral angle is 30º and $\mathbf{C}_h$ is [n,n] for armchair nanotubes. Chiral SWNTs have $\mathbf{C}_h$ = [n,m] where n is not equal to m, and a chiral angle which is greater than 0º and less than 30º. The electronic properties of nanotubes depend greatly on their structure. For example, it is known that [n,m] nanotubes are metallic if [2n + m] is a multiple of 3 and that other nanotube structures are semiconducting (Saito *et al.,* 1992).

These unique structures lead to unique SWNT properties—mechanical strength greater than that of Fe, density lower than that of Al, and thermal stability at 1400°C in a vacuum. The SWNTs emit electrons from their tips when exposed to a low electric field, enabling their application in flat-panel displays, transistor and novel data storages (Sander *et al*., 1998). In this system, H atoms would be designated as 0 and F atoms as 1. A tip that can distinguish between 0 and 1 rapidly and unambiguously is being investigated. In addition, a novel data storage system capable of 10^{15} bytes/cm^2 is being explored while an old data silicon-based storage system is at 10^8 bytes/cm^2. Their thin needle-like structure allows them to be used as probe tips in scanning tunneling microscopy and atomic force microscopy. The nanometer-scale spaces inside and among the SWNTs should provide large gas-adsorption capacities, which

are especially exciting when we consider hydrogen adsorption. A practical means of storing hydrogen will be a benefit for fuel-cell development and an important step towards achieving a source of clean energy that can be widely applied. A recent report has claimed that 10-wt% hydrogen uptake by SWNTs is possible (Lan *et al.,* 2005). Elsewhere, SWNTs with a diameter of about 0.4 nm—the thinnest yet—have been made (Dai *et al.,* 2001; Chen *et al*., 1998; 2001) and such fine SWNTs raise new possibilities for electrical superconductivity (Tang *et al.,* 2001) that could have a great impact as the critical temperature for superconductivity becomes higher. Another intriguing possibility is that we can use the hollow space inside SWNTs as one-dimensional fields for applications in physics, chemistry, and, perhaps in the future, biology.

Furthermore, the SWNTs can be capped at each end by joining the two hemispheres of a [60]-fullerene molecule with the ends of a cylindrical tube of the same diameter (Wang *et al.,* 2000; Tang *et al.,* 2001; Saito *et al.,* 1992). If the [60]-fullerene molecule is bisected normally to a 5-fold axis, the capped armchair tube can be obtained. On the other hand, if the [60]-fullerene molecule is bisected normally to a 3-fold axis, the capped zigzag tube can be generated (Yoshitake *et al.,* 2002). In addition, the reactivity of the C-C double bonds at the fullerene hemisphere cap ends of SWNTs is higher than the graphene-like sidewalls of SWNTs. This is due to the higher curvature of the capped end carbon nanotubes. The curvature can be measured as the pyramidal angle (θ_p), $\theta_p=(\theta_{\sigma\pi}-90)°$ where $\theta_{\sigma\pi}$ is an angle between the π-orbital and the σ-orbital of the carbon atom on SWNTs, which are 11.55°, 5.97°, and 5.78° for [60]-fullerene, sidewall of [5,5] and [9,0] SWNTs, respectively (Yumura *et al.,* 2004). From these values, its chemical reactivity trend can be predicted. Generally, the higher pyramidal angles, the higher reactivity and, therefore the cap sites are more reactive than another site.

However, the insolubility and high chemical stability obstruct the purification and impede the application of the nanotubes for certain purposes (Niyoki *et al.,* 2002; Sun *et al*., 2002; Stanislaus, *et al*., 1998). The key to solve this problem may be the chemical functionalization of CNTs by introducing new physical and chemical properties and increasing solubility. A number of simple organic reactions for the functionalization of the carbon nanotubes have been reported, such as the 1,3-dipolar cycloadditions (Lu *et al.,* 2003), the retro-cycloaddition reaction (Martin *et al.,* 2006), the ozonization (Lu *et al.,* 2002), the oxycarbonyl nitrene cycloaddition (Holzinger *et al.,* 2003), the Diels-Alder reaction (Lu *et al.,* 2002), the Bingel reaction (Coleman *et al.,* 2003), the dichlorocarbene addition (Hu *et al.,* 2003), the dipyridyl imidazolidene (Kang *et al.,* 2004), the addition of 2-carboxyethyl or 3-carboxypropyl addition (Peng *et al.,* 2003), and the fluorine addition (Cioslowski *et al.,* 2002). One of the most facile organic reactions, the 1,3-dipolar cycloadditions of ozone with SWNTs may offer a good way to improve solubility and the chemical reactivity of nanotubes. Moreover, it may be a common way to oxidatively break C-C double bonds at the cap of SWNTs to utilize in specific purposes, i.e., nanotubes molecular transporters (Bahr *et al.,* 2002; Kam *et al.*, 2004), molecular sieve (Hamada *et al.,* 1992) and hydrogen storage (Lee *et al.,* 2001; Dai *et al.,* 2002; Zhang *et al.,* 2003; Bacsa *et al.,* 2004; Lan *et al.,* 2005), because the ozonolysis of [60]-fullerene have been carried out by infrared spectroscopy detecting CO, CO_2, ester and quinone which are fragments from ozone oxidation at room temperature (Gillies *et al.,* 1988). At the same time, an unstable intermediate ($C_{60}O$) has been detected and isolated in the reaction of ozone with [60]-fullerene in solution by UV-vis spectroscopy (McKee *et al.,* 1981). From experimental evidence, the activation energy of 1,3-dipolar cycloadditions of ozone with ethylene is equal to 5 kcal/mol (Neeb *et al.,* 1998) that is the smallest activation energy for 1,3-dipolar cycloadditions comparing with other 1,3-dipolar molecules (nitrile

imine, nitrile ylide, nitrile oxide, diazomethane, methyl azide azomethine ylide and nitrone).

Recently, the FTIR studies of the oxidation of [60]-fullerene using ozone have been reported at room temperature (Mawhinney *et al.,* 2000). Two different surfaces bound functional groups, esters and quinines, as well as CO_2 and CO, were observed during the reaction. In addition, an unstable intermediate ($C_{60}O$) has been detected and isolated in the reaction of ozone with [60]-fullerene in solution by UV-vis spectroscopy (Mawhinney *et al.,* 2000). At the same time, the ozonolysis reaction of SWNTs was established and found to preferentially occur at the fullerene hemisphere of the capped nanotubes rather than at the sidewalls, producing the oxygenated species as found in the case of [60]-fullerene (Heymann *et al.,* 1994). The latter finding can be generally understood in terms of the relative curvature of the cap sites and the sidewalls. Nevertheless, recently, theoretical investigation concerning the ozonization of the sidewalls of small diameter SWNTs has revealed that the reaction is facile with only a small activation barrier (Lu *et al.,* 2000; 2003).

To our knowledge, the ozonization reaction on the fullerene hemisphere of the capped nanotubes has not yet been reported theoretically. Very recently, Iijima *et al.* have performed the density functional theory (DFT) on the study of the geometrical features of the finite-length carbon nanotubes capped with fullerene hemisphere (Yumura *et al.,* 2004). Their results showed that the geometries of the [5,5]-armchair nanotube series depended on the number of cyclic polyene units, but remained unchanged in the case of the [9,0]-zigzag nanotube series. With increasing nanotube length, the gaps between the highest-occupied molecular orbital (HOMO) and the lowest-unoccupied molecular orbital (LUMO) in the armchair series decreased with an oscillating manner. In contrast, the gaps for the zigzag series decreased with no oscillatory behavior with the increasing number of chains. These findings are rather

encouraging to find out whether the chemical reactivity of the end caps, fullerene hemisphere, of the capped SWNTs is sensitive to the nanotube length.

Therefore, in this study, we focus on the 1,3-dipolar cycloaddition reaction of ozone at the fullerene hemisphere cap ends of the [5,5] armchair SWNTs (C_{40+20n}, n=1.5-8.0) and the [9,0] zigzag SWNTs (C_{60+18n}, n=1-8) using the two-layered ONIOM (B3LYP/6-31G(d):AM1) and PBE/def-SV(P) methods, with the aims to determine the influences of the finite length of the SWNTs on its chemical reactivity and to compare chemical reactivity of the cap-ended [5,5] armchair SWNT and the cap-ended [9,0] zigzag SWNT.

LITURATURE REVIEW

Iijima, (1991) prepared a novel type of finite carbon structure consisting of needle-like tubes known as carbon nanotubes (CNTs). Using the arc-discharge evaporation method, similar to that used for fullerenes synthesis, these tubes grew at the negative end of the electrode used for the arc discharge. Transmission electron microscopy (TEM) revealed that each tube comprised coaxial tubes of graphitic sheets, ranging from 2 to about 50. On each tube, the C-atom hexagons were arranged in a helical fashion about the needle axis. The formation of these needles ranged from a few to a few tens of nanometers in diameter. Ajayan *et al.,* (1993) described experiments in which annealing of the tubules in the presence of liquid led to the opening of the capped tube ends and subsequent filling of the tubes with molten material through capillary action (Ebbesen *et al.,* 1992). The nanotubes thus acted as moulds for the fabrication of (possibly metallic) wires, some of which were less than two nanometres in diameter. They, at the same time, had presented evidence through high-resolution electron microscopy images for the open-end growth of carbon nanotubes. The nucleation of positive (pentagons) and negative (heptagons) disclinations on open tube ends resulted in changes of growth directions, producing different morphologies. Iijima *et al.,* (1993) synthesized single-shell tubes with diameters of about 11 nm, which grew in the gas phase. Electron diffraction from a single tube confirmed that the helical arrangement of C hexagons similar to those observed previously for multi-shell tubes. In addition, they had synthesized abundant single-shell tubes with diameters of about one nanometer. In 1997, SWNTs became the prospect of both new fundamental science and useful nanotechnological applications. High yields (70–90%) of SWNTs close-packed in bundles can be produced by laser ablation of carbon targets. The electric-arc technique used to generate fullerenes and multi-walled nanotubes was cheaper and easier to implement,

but previously had led to only low yields of SWNTs (Journet *et al.,* 1997). Odom *et al.*, (1998) had found that the semiconducting and metallic behavior of SWNTs depend inversely on their diameter. This was confirmed again by Yamashita *et al.,* (1999) and by Venerma *et al.*, (2000). Furthermore, Zhou *et al.,* (2000) summarized some of their recent studies on the material properties of SWNTs. They described experiments on the synthesis of SWNTs with controlled molecular structures and assembly of functional *macroscopic* structures. Besides, they presented results on the electron field emission properties of macroscopic SWNTs cathodes. Alternatively, Niyoki *et al.,* (2000) considered carbon nanotubes as a new macromolecular form of carbon with unique properties and with great potential for practical applications. They showed that carbon nanotubes might take on properties that were normally associated with molecular species, such as solubility in organic solvents, solution based chemical transformations, chromatography, and spectroscopy.

Carbon nanotube synthesis by CVD involves heating a catalyst material in a furnace and flowing a hydrocarbon gas through the tube reactor for a period of time. The catalytic species are transition-metal nanoparticles typically supported on high surface area materials, such as alumina (Dai *et al.*, 2001). Simplistically, the catalyst particles serve as seeds to nucleate the growth of nanotubes. They have developed patterned growth approaches to obtain organized nanotube structures. The idea is to position a catalyst in arrayed fashions for the growth of nanotubes from specific catalytic sites on surfaces (Kong *et al.,* 1993). They have carried out such patterned growth for both multi-walled and single-walled nanotubes, exploited ways including self-assembly and active electric field control to manipulate the orientation of nanotubes, and pursued several generations of catalysts ranging from powdery supported catalyst to discrete catalytic nanoparticles. These works have led to

ordered nanotube arrays or networks formed at the synthesis stage of nanotubes.

The covalent chemistry of single-wall carbon nanotubes have been considerably focused on the outer surface of SWNTs. The covalent attachment of carbon nanotubes was anticipated to facilitate applications development by improving solubility and ease of dispersion, and providing for chemical attachment to surfaces and polymer matrices. While it was clear that more investigation was needed to elucidate the nature and locality of covalently attached nanotubes, developments to date indicate that carbon nanotubes may indeed be considered a true segment of organic chemistry (Bahr *et al.,* 2002). Alkyl lithium reagents were used to attach alkyl groups to the sidewalls of fluoro nanotubes. Thermal gravimetric analysis combined with UV-vis-Nir spectroscopy had been used to provide a quantitative measure of the degree of functionalization. SWNTs prepared using the high pressure carbon monoxide (HiPco) process exhibited a higher degree of alkylation than SWNTs from the laser-oven method, indicating that the smaller diameter fluoro tubes were alkylated more readily. The spectral signature of the pristine SWNTs can be regenerated when the alkylated SWNTs were heated in Ar at 500°C, demonstrating that dealkylation occurred at this temperature (Saini *et al.,* 2003; Ying *et al.,* 2003). Characterization of chemically modified carbon nanotubes has been achieved using ^{13}C nuclear magnetic resonance (NMR) spectroscopy (Ruther *et al.,* 2004).

The electronic properties of SWNTs have been studied by many theoretical investigators. Cioslowski *et al.*, (2000) computed standard enthalpies of formation, ionization potentials, electron affinities, and band gaps of the finite-length [5,5] and [9,0] SWNTs capped with fullerene hemispheres by using the B3LYP/6-311G(d) level of theory. Properties of SWNTs were

found to depend strongly on the tube length and, in the case of the [9,0] zigzag species, on the relative orientation of the caps. The metallic character of an uncapped infinite length [5,5] SWNTs manifested itself in the oscillatory dependence of the properties of capped finite length tubes on their size. An infinite-length [9,0] SWNTs was predicted to be a semiconductor rather than a metal irrespective of the presence of caps. The results emphasized the slow convergence of SWNTs properties with respect to the tube length and uncovered small but significant radial distortions along the long axes of SWNTs. Iijima *et al.*, (2004) showed that the structures of the finite-length [5,5] and [9,0] SWNTs capped with fullerene hemisphere were analyzed by quantum chemical calculations at the B3LYP level of theory demonstrated that the geometries of the armchair tubes depended on the number of cyclic *cis*-polyene chains lined up along the tube axis, while the zigzag tubes consisted of Kekule-type networks in the cylinder, the geometries being independent of the number of component cyclic *trans*-polyene chains. Zhou *et al.*, (2004) computed all-electron static and time-dependent DFT electronic calculations, with complete geometrical optimization, performed on tubular molecules up to $C_{210}H_{20}$ that were finite sections of the [5,5] armchair-SWNTs with hydrogen termination at the open ends. They found C-C bond reconstruction at the tube ends. This initiated bond alternation that propagated into the tube centers. A small residual C-C bond alternation and band gap might be found in the infinite tube. The HOMO-LUMO gap and the lowest singlet excited state, whose energies showed a periodicity with length as previously calculated, were optically forbidden. However, the ionization potential, electron affinity, chemical hardness, and relative energetic stability all showed the length periodicity in the HOMO-LUMO gap.

The reactivity of the fullerenes is primarily driven by the enormous strain engendered by their spherical geometry as reflected in the

pyramidalization angles of the carbon atoms (Haddon, 1993). For an sp^2-hybridized (trigonal) carbon atom, planarity is strongly preferred, and this implies a pyramidalization angle of $\theta_P = 0°$, whereas an sp^3-hybridized (tetrahedral) carbon atom requires $\theta_P = 19.5°$ (Figure 4a). All of the carbon atoms in [60]-fullerene have $\theta_P = 11.6°$, and it is immediately clear that their geometry is more appropriate for tetrahedral than trigonal hybridization. Thus the chemical conversion of any trivalent carbon atom in [60]-fullerene to a tetravalent carbon atom relieves the strain at the point of attachment and mitigates the strain at the 59 remaining carbon atoms (Haddon, 1993). Hence reactions that serve to saturate the carbon atoms are accelerated by strain relief, and this strongly favors fullerene addition chemistry (Haddon, 1993; Taylor *et al.*, 1993).

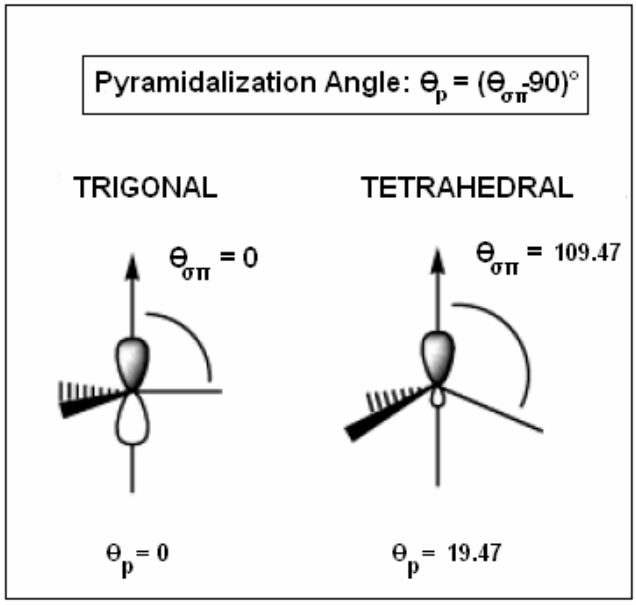

(a)

Figure 4 Diagrams of (a) pyramidalization angle (θ_P), and (b) the π-orbital misalignment angles (Φ) along the C1-C4 in the [5,5] SWNT and its capping [60]-fullerene.

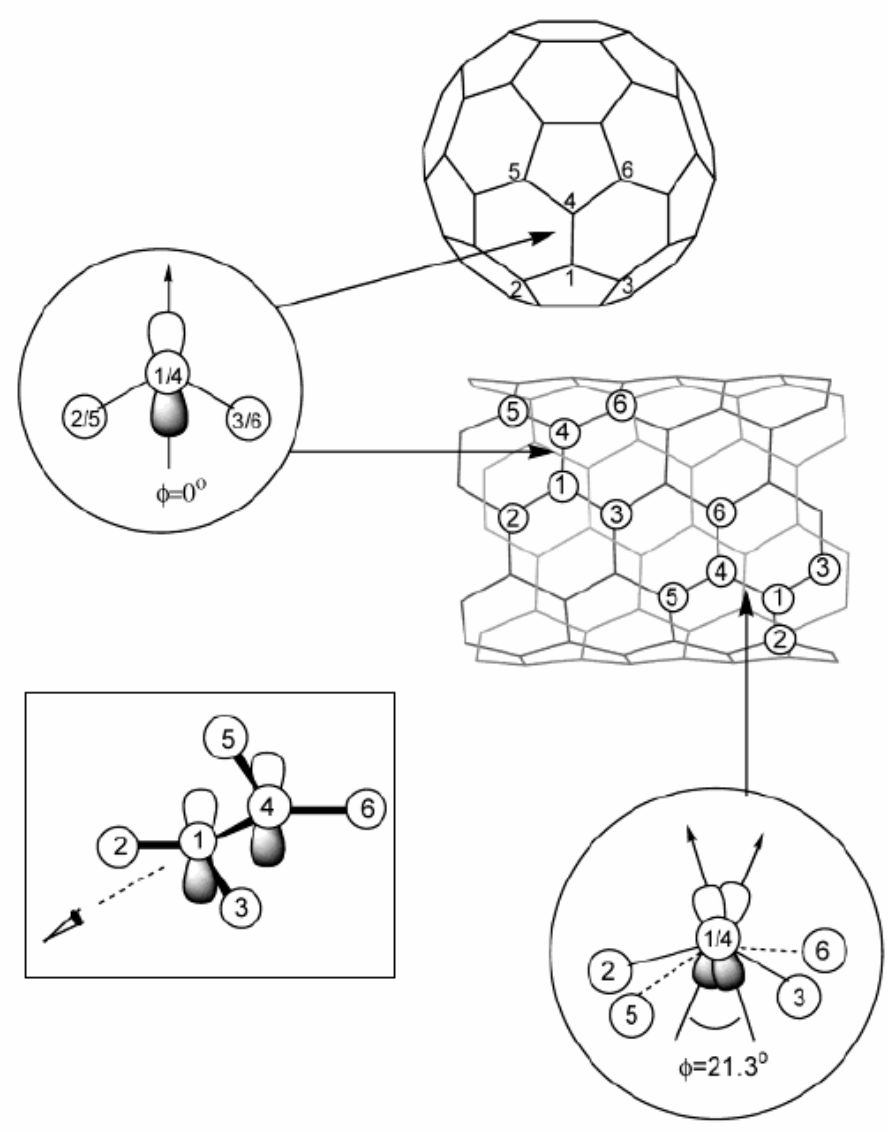

(b)

Figure 4 (Cont'd)

The curvature-induced pyramidalization and misalignment of the π-orbitals (Hamon, *et al.,* 2001; Chen, *et al.,* 1998; Haddon, 1993) of the carbon atoms induces a local strain (Figure 4b), and carbon nanotubes are expected to be more reactive than a flat graphene sheet. From the standpoint of the chemistry, it is conceptually useful to divide the carbon nanotubes into two regions: the end caps and the side wall. The end caps of the carbon nanotubes resemble a hemispherical fullerene, and because it is impossible to reduce the

maximum pyramidalization angle of any fullerene below about θ_P max = 9.7°, (Haddon, 1997) this ensures that the end caps will always be quite reactive, irrespective of the diameter of the carbon nanotube. In the [5,5] SWNT, which is capped by a hemisphere of [60]-fullerene, the pyramidalization angles are as follows: θ_P = 11.6° (end cap) and θ_P = 6.0° (side wall) (Hamon, *et. al.,* 2001).

A few theoretical works (Hamada *et al.,* 1992; Saito *et al.,* 1992; Mintmire *et al.,* 1992) predicted that the electronic properties of "ideal" carbon nanotubes depend on the width of the graphene sheet (diameter of the tube) and the way it is folded (chirality of the tube), which are both functions of [n,m]. The electronic properties of a nanotube vary in a periodic way between being metallic and semiconductor and follows a general rule: if (n - m) is a multiple of 3, then the tube exhibits a metallic behavior (finite value of carriers in the density of states at the Fermi energy); if (n - m) is not a multiple of 3, then the tube exhibits a semiconducting behavior (no charge carriers in the density of states at the Fermi energy). Five years later, using scanning tunneling microscope probes at low temperature, (Wildoer *et al.,* 1998; Odom *et al.,* 1998) experimentalists measured the electronic structure (density of electronic states, DOS) and physical structure (the nanotube diameter and helicity, which are directly related to [n,m]), confirming the theoretical predictions. Sharp peaks (van Hove singularities) in the DOS, which are the characteristic signature of the strongly one-dimensional nature of the conduction within a 1D system, were also observed and compared to the theoretical models.

For doping carbon nanotubes, boron doping can be carried out by growing tubes in a carbon arc using a BN-rich consumable anode (Carroll *et al.,* 1998). On the other hand, nitrogen-doped carbon nanotubes can be synthesized by pyrolyzing ferrocene/melamine mixtures at elevated temperatures (Czerw *et al.,* 2001). Changes in the electronic structure of carbon nanotubes due to the introduction of boron and nitrogen in the lattice have been

identified using scanning tunneling spectroscopy (Carroll *et al.,* 1998; Czerw *et al.,* 2001). Both boron- and nitrogen-doped tubes are metallic with no apparent band gap, in contrast to undoped tubes with varying electronic character. However, in both cases, the local density of states (LDOS) exhibit either strongly localized acceptor states (p-doping) or donor states (n-doping) near the Fermi level. First principles calculations show that changes in the LDOS of boron-doped tubes, (Carroll *et al.,* 1998) as determined from tunneling microscopy, must be interpreted in terms of nanodomains of BC_3 islands. However, pyridine-like N structures are responsible for the metallic behavior and the strong electron donor states observed near the Fermi level in the LDOS of nitrogen-doped tubes (Czerw *et al.,* 2001). The temperature-dependent thermoelectric power of boron- and nitrogen-doped carbon nanotubes have been measured, showing that such dopants can be used to modify the majority carrier conduction from p-type to n-type. These electrons-(hole)-rich structures are examples of n-type (p-type) nanotubes, which could again pave the way to real molecular heterojunction devices (Choi *et al.,* 2000). As noted above, oxidative doping during nitric acid purification exerts a noticeable effect on the electronic transitions seen in the SWNTs. Similar effects may be observed by doping solutions of the nanotubes with halogens (Chen *et al.,* 1998; Hamon *et al.,* 1999). Under saturation doping, bromine and iodine completely deplete the electrons from the valence band responsible for the singlet transition in the semiconducting nanotubes. Similar results were obtained under electrochemical cycling (Petit *et al.,* 1999) and by controlled doping of thin films of carbon nanotubes (Kazaoui *et al.,* 1999; 2001). Furthermore, solid state doping with halogens has been shown to influence the conductivity of SWNTs.

The functionalization of SWNTs has been highlighted by various investigators around the world. Experimental and theoretical studies have been employed to understand their kinetics and thermodynamics properties.

Khabashesku *et al.,* (2000) had utilized direct fluorination for the preparation of fluoronanonotubes and their subsequent derivatization (Mickelson *et al*., 1998). The results proved that the addition of fluorine drastically enhanced the reactivity of the nanotube side walls. The use of this strategy as a versatile tool for preparation and manipulation of SWNTs with variable side-wall functionalities was demonstrated. The functionalized SWNTs showed an improved solubility in selected solvents and significantly altered electrical, mechanical, and optical properties. At the same time, there are two groups interested in ozonization reaction of [60]-fullerene. The first group showed an unstable intermediate, detected and isolated in the reaction of ozone with [60]-fullerene in solution. On the basis of its UV-vis absorption spectrum, the intermediate was identified as $C_{60}O_3$, a primary ozonide. This 6/6-closed adduct of ozone with [60]-fullerene thermally dissociated to $C_{60}O$ plus O_2 in toluene solution, octane solution, and the solid phase with rate constants (at 23 °C) of 4.6×10^{-2}, 1.3×10^{-3} and 3.0×10^{-3} min^{-1}, respectively. The activation energy for dissociation in toluene solution was approximately 89 kJ/mol. AM1 calculations indicated that the formation and subsequent dissociation of $C_{60}O_3$ were both exothermic processes (Heymann *et al.,* 2000). The second group showed that semi-empirical molecular orbital calculations can be carried out on the ozonization of [60]-fullerene in order to obtain information on possible reaction paths and products. The computational results showed that not only from a thermodynamic point of view but also from a kinetic point of view the O_3 was most likely added on the 6/6C-C of [60]-fullerene. In the ozonization reaction, the major product was $C_{60}O$ with epoxide functionality (Hu *et al.,* 2003). After that, Lu and co-workers investigated ozonization of the sidewalls of SWNTs by means of two-layered ONIOM(B3LYP/6-31G(d):AM1) calculations. The theoretical calculations revealed that the 1,3-dipolar cycloaddition of ozone onto the sidewalls of [5,5] SWNTs was site-selective and facile with a small activation barrier of 1.4 kcal/mol without BSSE

correction. The desorption of oxygen from the ozone adduct was found to be favorable over the decomposition process that gave rise to the epoxy adduct and O_2 upon thermal activation. This work implied the possibility of functionalizing the sidewalls of SWNTs by means of 1,3-dipolar cycloadditions of 1,3-dipolar molecules (Lu *et al.,* 2002; Zhu *et al*., 2003). In addition, this group focused on that the 1,3-dipolar cycloadditions of a series of 1,3-dipolar molecules (azomethine ylide, ozone, nitrone, nitrile imine, nitrile ylide, and nitrile oxide, diazomethane, and methyl azide) onto the sidewalls of carbon nanotubes was assessed theoretically by means of a two-layered ONIOM approach. The theoretical calculations predicted that the reactivity was moderately dependent on the diameters of SWNTs, implying the feasibility of making use of the heterogeneous 1,3-dipolar cycloadditions chemistry to purify and separate SWNTs diameter-specifically (Lu *et al.,* 2003). From 2003 to 2004, Prato, one of many experimental researchers, showed that the organic functionalization of carbon nanotubes has opened new avenues with opportunities to fabricate novel nanostructures by improving both their solubility and properties. The 1,3-dipolar cycloaddition of azomethine ylides onto carbon nanotube (CNT) networks may play a relevant role towards this direction. CNT-based materials have been synthesized possessing differently functionalized solubilizing chains and hold strong promise as useful building blocks for the construction of novel hybrids for nano- and bio-technological applications (Georgakilas *et al.,* 2002; Bianco *et al.,* 2005). Presently, Limtrakul and co-workers have presented the Diels-Alder cycloadditions of single-wall carbon nanotubes with electron-rich dienes and found that the reactivity of the Diels-Alder reaction has been correlated to the distance between the methylene carbons in the butadiene moiety (R1,4) of these outer-ring dienes. The reactivity is higher as the R1,4 becomes shorter (Warakulwit *et al.,* 2005).

Functionalization and interfacing with biological systems are an important aspect of the chemistry of nanotube "macromolecules" (Chen *et al.,* 1998; Boul *et al.,* 1999; Star *et al.,* 2001; Ouyang *et al*., 2002; Hirsch, 2002). As mentioned, however, covalent sidewall functionalization of nanotubes from the sp^2 to sp^3 structure is both difficult and undesired because of the loss of conjugation (Boul *et al.,* 1999). Alternatively, it is possible to functionalize SWNTs noncovalently (O'Connell *et al.,* 2001; Chen *et al.,* 2001) to preserve the sp^2 structures and their electronic properties that are useful for various post functionalization applications. Nanotube functionalization and bioimmobilization are motivated by the recent activities in biological applications of novel solid-state nanomaterials. The unique physical properties of molecular-scale or nanoscale solids (dots or wires), when utilized in conjunction with the remarkable biomolecular recognition capabilities, could lead to miniature biological electronic devices, including probes and sensors. The interface between biological molecules and nanomaterials is critical to such applications. With nanotubes, such exploration is still in its early stage, with wide open room and many possibilities (Dai, 2002).

MATERIAL AND METHOD

1. Theoretical background

From time to time, people have tried to understand nature in order to increase their lifespan and so forth. The best way to explore the laws of nature is by doing experiments; however, one of their limitations is that it is hard to conduct on nanoscale systems involving the interactions of electron-electron, electron-nucleus, and nucleus-nucleus within atoms or molecules. Therefore, in these cases, calculations based on mathematical models can be helpful to increase the useful knowledge and understanding of microscopic phenomena.

With the fundamental laws of both quantum mechanics and molecular mechanics, the great number of different calculation techniques and even more calculation software of varying quality were used. At the present time, the information technology (IT) revolution has provided faster and cheaper computer systems for performance computers. This has led to the tremendous increase of computer-based calculations in the field of nanoscal science, which plays a key role in the atomic and molecular scales. Computer based calculations have a corollary for predicting the electronic and chemical properties of nanoscal materials, especially the one-dimensional structure of [60]-fullerene, and two-dimensional structure of carbon nanotubes.

Computational chemistry has to be applicable to a certain system size or the number of atoms or basis functions per molecule. In this work, we have dealt with a large system, where the basis function of the largest model is over 4,000 functions; hence, in order to get the structural and energetic information of carbon nanotubes, the choice of the methods has to be carefully considered.

1.1 The Our own N-layered Integrated molecular Orbital molecular Mechanics (ONIOM)

ONIOM is one of the hybrid methods between quantum mechanics (QM) and molecular mechanics (MM) (Dapprich, *et al.*, 2003) that enables different levels of theory to be applied to different parts of a molecule and combined to produce a consistent energy expression. The objective is to perform a high-level calculation on just a small part of the system and to include the effects of the remainder at lower levels of theory, with the end result being of similar accuracy to a high-level calculation on the full system. In addition, the ONIOM method is based on the principle of the extrapolation and is conceptually quite different, although operationally similar in some special cases, from the QM/MM methods. Originally, the MO and the MM methods were combined under the name of the integrated molecular orbital-molecular mechanics (IMOMM). Later the method was further expanded to an onion-like multi-layered method, ONIOM, with ONIOMn referring specifically to an n-layered version, and individual methods used are divided by a colon, such as ONIOM2(MP2:MM3). Hence, IMOMM is equivalent to ONIOM2 (MO:MM) and IMOMO to ONIOM2(MO:MO). The ONIOM method has been implemented into the Gaussian03 program system (Frisch *et al*., 2003).

Also, the ONIOM scheme had been proved to be power tools for the theoretical treatment of large molecular systems, such as carbon nanotubes (Lu *et al.,* 2001; 2003; Warakulwit *et al.,* 2005) and zeolites (Namuangruk, *et al.,* 2004; 2005) where the different levels of theory are applied to different parts of a molecule. Within the framework, the modified handling of the like atoms is introduced to terminate the dangling bonds of the model system.

The basic idea behind the ONIOM approach can be explained most easily when it is considered as an extrapolation scheme in a two-dimensional space, spanned by the size of the system on one axis and the level of theory on the other axis. Figure 5 shows the extrapolation procedure schematically. The goal is to describe the real system at the higher level of the theory, i.e., the approximation of the target E_4 (point 4) in a system partitioned into the two-layered ONIOM or E_9 (point 9) in a system consisting of the three layers. In the case of two layers, the extrapolated energy E_{ONIOM2} is then defined as:

$$E_{\mathrm{ONIOM2}} = E_3 - E_1 + E_2 \tag{1}$$

where E_3 is the energy of the entire (real) system calculated at the low-leveled method and E_1 and E_2 are the energies of the model system determined at the low and high levels of theory, respectively. E_{ONIOM2} is an extrapolation to the true energy of the real system E_4:

$$E_4 = E_{\mathrm{ONIOM2}} + D \tag{2}$$

Hence, if the error D of the extrapolation procedure is constant for two different structures (e.g. between reactant and transition state), their relative energy ΔE_4 will be evaluated by using the ONIOM energy $\Delta E_{\mathrm{ONIOM2}}$.

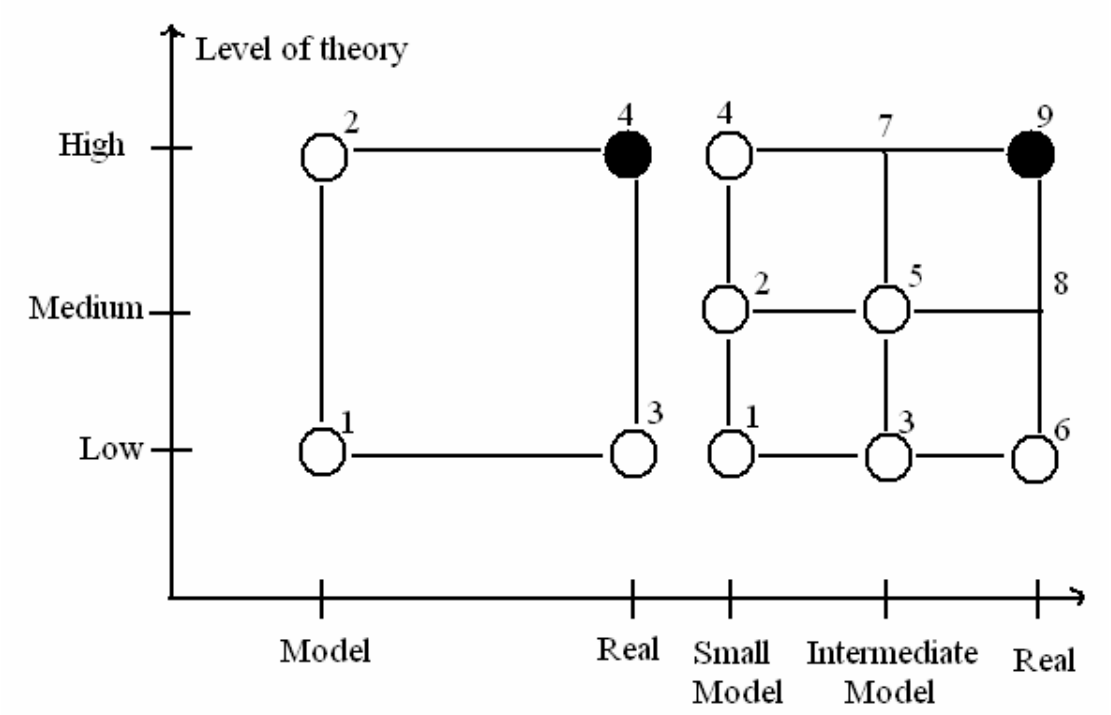

Figure 5 The ONIOM extrapolation scheme for a molecular system partitioned into two (left) and three (right) layers.

For a system partitioned into three different layers, the expression for the total energy E_{ONIOM3} as an approximation for E_9 reads:

$$E_{\mathrm{ONIOM3}} = E_6 - E_3 + E_5 - E_2 + E_4 \tag{3}$$

Since the evaluation of E_1 (the smallest model system at the lowest level of theory) does not require much computational effort, its value can be used to determine the effect of the three-layer approach as compared to a two-layer partitioning with points 1, 4, and 6. If the energy difference between the two- and three-layered extrapolation is constant, a two layer partitioning with the intermediate layer omitted would give comparably accurate results.

It should be noted that the layers need not be inclusive or contiguous. The so-called ‘inner layer’ does not have to be physically inside the ‘outer

layer'. The layers can be any part of the system. Each layer does not have to be contiguous; it can consist of several separate regions of the system.

1.2 Perdew-Burke-Ernzerhof (PBE) method

Perdew-Burke-Ernzerhof (PBE) method is one of nonempirically generalized gradient approximations (GGA's) for the exchange-correlation energy. It has been used to improve the local spin density (LSD) description of atoms, molecules, and solids. Perdew, Burke, and Ernzerhof presented a simple derivation of a simple GGA in 1996 (Perdew, *et al*., 1996), in which all parameters (other than those in LSD) were fundamental constants.

Also, the goal of the PBE method was to present a simple, nonempirical derivation of a simplified generalized gradient approximation (GGA) for the exchange-correlation energy of the density functional theory. Among the many conditions that might have been imposed to construct the functional, they selected as most appropriate to the GGA form those already satisfied by the local spin density (LSD) approximation. Only the exchange-correlation energy $E_{\mathrm{XC}} = E_{\mathrm{X}} + E_{\mathrm{C}}$ as a functional of the electron spin densities $n_{\uparrow}(r)$ and $n_{\downarrow}(r)$ must be approximated. The most popular functionals have a form appropriate for slowly varying densities: the LSD approximation

$$E_{XC}^{LSD}\left[n_{\uparrow}, n_{\downarrow}\right] = \int d^3 r n \varepsilon_{XC}^{unif}(n_{\uparrow}, n_{\downarrow}) \tag{4}$$

where $n = n_{\uparrow} + n_{\downarrow}$, and the PBE approximation

$$E_{XC}^{PBE}\left[n_{\uparrow}, n_{\downarrow}\right] = \int d^3 r f(n_{\uparrow}, n_{\downarrow}, \nabla n_{\uparrow}, \nabla n_{\downarrow}) \tag{5}$$

In comparison with LSD, PBE approximation tends to improve total energies, atomization energies, energy barriers, and structural energy

differences. The PBE approach, like other GGA methods, expands and softens bonds, an effect that sometimes corrects and sometimes overcorrects the LSD prediction. Typically, generalized gradient approximations favor density inhomogeneity more than LSD does.

To facilitate practical calculations, ε_{XC}^{unif} and f must be parametrized analytic functions. The exchange-correlation energy per particle of a uniform electron gas, ε_{XC}^{unif}, was well established by Perdew and Wang in 1992, but the best choice for $f(n_\uparrow, n_\downarrow, \nabla n_\uparrow, \nabla n_\downarrow)$ was still a matter of debate. Judging the deviations and formal properties of the PBE approximation or other GGA's could guide a rational choice among them. A first-principles numerical GGA could be constructed by starting from the second-order density-gradient expansion for the exchange-correlation hole surrounding the electron in a system of slowly varying density, then cutting off its spurious long-range parts to satisfy sum rules on the exact hole.

The PBE approximation proposed (Perdew, et al., 1996) retained correct features of LSD, and combined them with the most energetically important features of gradient-corrected nonlocality. It would, in addition, exact for the uniform electron gas and very useful for solids, such as carbon nanotubes.

2. Aromaticity and Nucleus Independent Chemical Shift (NICS) Analysis

The rule of aromaticity or Huckel's rule defined that aromatic molecules must be cyclic and planar. Also, each atom of the ring must have a p orbital and these p orbitals must be perpendicular to the plane of the ring. Such molecules must, in addition, contain 4n+2 pi electrons (where n = 0, 1, 2, …). It is also noted that nucleus independent chemical shifts (NICS) have been used extensively for the identification of aromaticity properties of molecules, ions,

intermediates, and transition states since their introduction in 1996 by Schleyer and coworkers.

2.1 Aromaticity

A molecular orbital description of benzene provides a more satisfying and more general treatment of aromaticity. We know that benzene has a planar hexagonal structure in which all the carbon atoms are sp^2 hybridized, and all the carbon-carbon bonds are equal in length. The ability to sustain a diatropic ring current is the defining characteristic of aromatic species. Cyclic electron delocalization results in enhanced stability, bond length equalization, and special magnetic as well as chemical and physical properties (Schleyer *et al.,* 1996). In contrast, antiaromatic compounds sustain paratropic ring currents despite their localized, destabilized structures (Sondheimer *et al.,* 1996). Furthermore, benzene rings may be joined together to give larger polycyclic aromatic compounds, such as coronene, corannulene, and graphene sheet, shown in Figure 6.

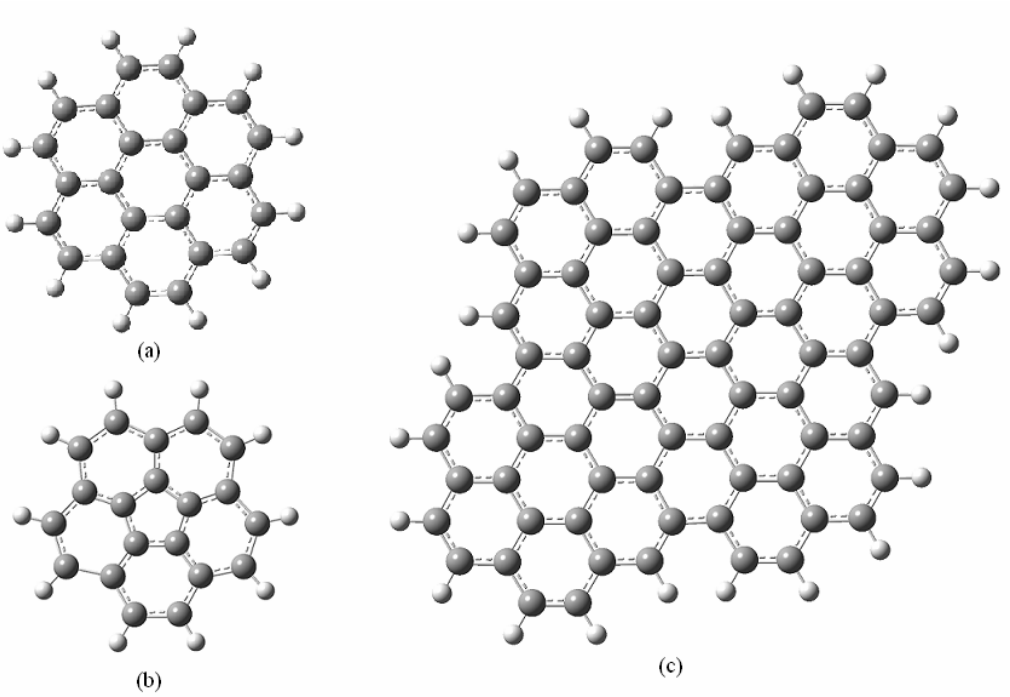

Figure 6 Some fused benzene ring compounds; (a) coronene, (b) corannulene, (c) graphene sheet.

If we extend the structure of corannulene, shown in Figure 6b, by adding similar cycles of five benzene rings, the curvature of the resulting molecule should increase, and eventually close into a sphere of carbon atoms. The archetypical compound of this kind ([60]-fullerene) has been named buckministerfullerene (Kroto *et al.,* 1985) because of its resemblance to the geodesic structures created by Buckminister Fuller. Otherwise, if we enroll a graphene sheet, shown in Figure 6c, we will get the carbon nanotubes, where their electronic properties depend on their diameter and chirality.

2.2 Nucleus Independent Chemical Shift (NICS) Analysis

One of the most powerful methods for predicting the aromaticity is a nuclear independent chemical shift (NICS) analysis (Schleyer *et al.,* 1996).

The NMR chemical shift is derived from the Larmor frequency of the nuclear spin of an atom, which describes the precession of the spin when the system is placed in a magnetic field. Since the electrons also react to the external field, the total magnetic field responsible for this precession is the superposition of the external one and the field induced by the electronic response. The nuclear shielding tensor is the negative proportionality factor between the electronically induced magnetic field, taken at the atomic position, and the externally applied one. The induced field and thus the chemical shift tensor, however, are well-defined in all points of space, not only at the positions of the nuclei. This generalization of the chemical shift into such a scalar field is called NICS. Also, NICS is defined as the negative value of the absolute magnetic shielding calculated at the ring centre. Initially, probes (bq's) were placed at the centers of systems (NICS(0)) and later, 1Å above the molecular planes (NICS(1)). The method is based on scanning NICS values over a distance and separating them into in-plane and out-of plane contributions. The shapes of the plots of the chemical shifts and their components as a function of the distance of the NICS probe (bq) from the molecular plane give a clear indication of diamagnetic and paramagnetic ring currents. This method is applied to several $(4n + 2)$- and $4n$ π-electron systems (molecules and ions) in the singlet and triplet electronic states, including some of the problematic systems mentioned above. It is also shown that relative aromaticities of rings in polycyclic systems (local aromaticities) cannot be estimated by comparing NICS or NICS-scan values. Moreover, Schleyer and his coworkers had established that NICS(1) provides appropriate information about the aromaticity of various hydrocarbons. Within this model, the aromatic rings were assumed to be the rings with negative values of NICS. The more the negative value of this descriptor the greater is the aromatic character of the molecular system (Elango *et al.*, 2005).

3. Details of Calculation

The 1,3-dipolar cycloadditions of ozone on the surface of [60]-fullerene and the caps of two series of [5,5] C_{40+20n} (n=1.5-8.0) shown in Figure 8 and [9,0] C_{60+18n} (n=1-8) single-walled carbon nanotubes capped with [60]-fullerene hemispheres shown in Figure 9 have been carried out with; (1) the density functional PBE approach (Eichkorn *et al*., 1995) together with the standard def-SV(P) basis set; (2) the two-layer Our own N-layered Integrated molecular orbital molecular Mechanics technique (ONIOM2) (Dapprich *et al.,* 1999). The hybrid density functional B3LYP (Becke *et al.,*1993; Lee *et al.,* 1988) together with the standard 6-31G(d) basis set and the Austin model one (AM1) method (Dewar *et al.,* 1977) were employed for the high-level and low-level treatments, respectively. The fully optimized geometries and the whole energies were performed by a PBE approach which existed in the TURBOMOLE package and an ONIOM (B3LYP/6-31G(d):AM1) approach using the Gaussian 03 package (Frisch *et al.,* 2003). The fullerene and its derivatives, the [5,5]-armchair and the [9,0]-zigzag cap of single-walled carbon nanotubes were taken and represented by [60]-fullerene, C_{150}-armchair, and C_{150}-zigzag model tubes (optimum diameter ≈ 6.80, 6.78, and 7.05 Å, respectively), which are the representatives of two series of nanotubes as portrayed in Figure 7, in which the high-level part contains 14 carbon atoms (see the ball and stick atoms in Figure 7a). In addition, the *cis*- and *trans*-cyclic polyenes are shown in the boundary dash line of Figure 7b and 7c, respectively.

The reaction in this work is focused on the naphthalene-like carbon-carbon double bond (C1-C2) merely because its π-orbital misalignment angles are equal to 0°, whereas the indene-like carbon-carbon double bond (C1-C3) is equal to 21.3° (Niyoki *et al.,* 2003). The π-orbital misalignment of carbon atoms induces a local strain leading to the C1-C2 double bond being more energetically reactive than the C1-C3 double bond. Therefore, the C1-C2

double bond at the cap end of the SWNT is the most active site and can be readily functionalized. Furthermore, in this study, the NICS(1) have shown that the C1-C2 double bond is far more dipolarophilic than the C1-C3 double bond (see Figure 7a).

The apparent activation energy (E_a) and the relative reaction energy (E_r) are defined as the energy between the isolated reactants and their transition state as well as between those and the local minimum adduct, respectively.

$$E_a = E(\text{transition state complex}) - E(\text{ozone}) - E(\text{nanotubes}) \quad (6)$$

$$E_r = E(\text{adduct}) - E(\text{ozone}) - E(\text{nanotubes}) \quad (7)$$

In order to obtain more reliable apparent activation energy (E_a), basis set super position error (BSSE) corrections were also taken in this work. It is known that the hybrid density functional (B3LYP) approach does not account for the dispersion component of the interactions. The discrepancy arises from a phenomenon known as BSSE; the wavefunctions of monomers are expanded in much fewer basis functions than the wavefunctions of the complexes. It is clear that the BSSE would be expected to be particularly significant when used in an adequate basis set, which do not provide for enough representation of the electron distribution far from the nuclei, particularly in the region where non-covalent interactions are strongest. One way to estimate the basis set superposition error widely employed is the counterpoise correction method in which the entire basis set is included in all calculations. The counterpoise corrected interaction energy (E_{CP}) between molecules A and B ($A+B \rightarrow AB$) molecule can be computed as:

$$E_{CP} = E(AB,r_c)^{AB} - E(A,r_r)^{AB} - E(B,r_r)^{AB} \quad (8)$$

The label r_c and r_r indicate the geometry of the complex and the isolated reactants, respectively. The superscript AB indicates that the complexes as well as the separated components are calculated in the same absolute basis functions or the number of basis wavefunctions. The calculation of the energy of the individual species A is performed in the presence of ghost orbitals of B, without the nuclei or electrons of B. The approximation to equation (8) for calculation of a counter point correction is

$$E_{CP} = E(AB,r_c)^{AB} - E(A,r_r)^{AB} - E(B,r_r)^{AB} + [E(A,r_c)^{A} - E(B,r_c)^{B} - E(A,r_c)^{AB}\, E(B,r_c)^{AB}] \quad (9)$$

where the superscripts A and B indicate that the separated components are calculated with their basis functions separately.

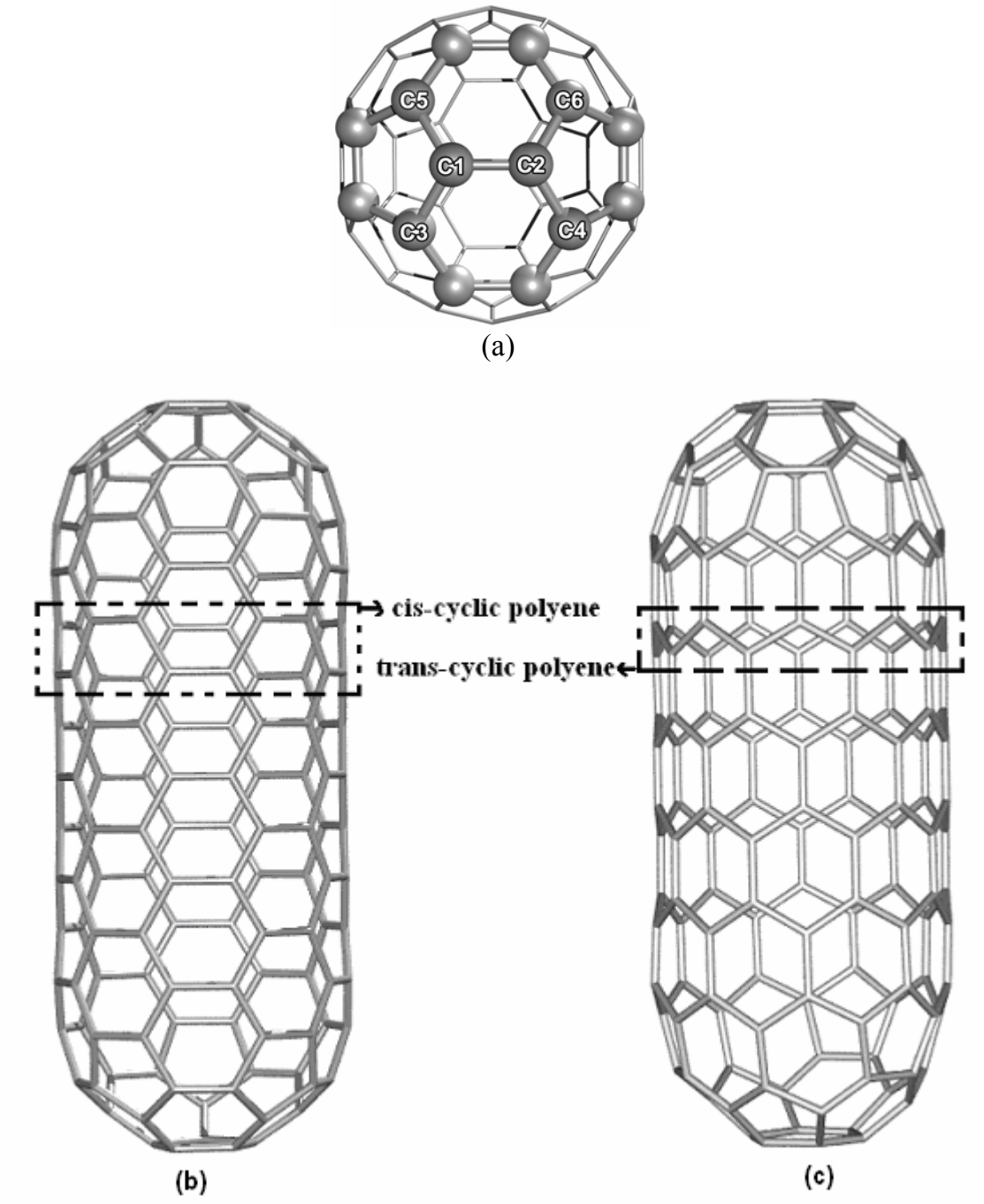

Figure 7 (a) [60]-fullerene; (b) C_{150}-armchair CNTs; (c) C_{150}-zigzag CNTs.

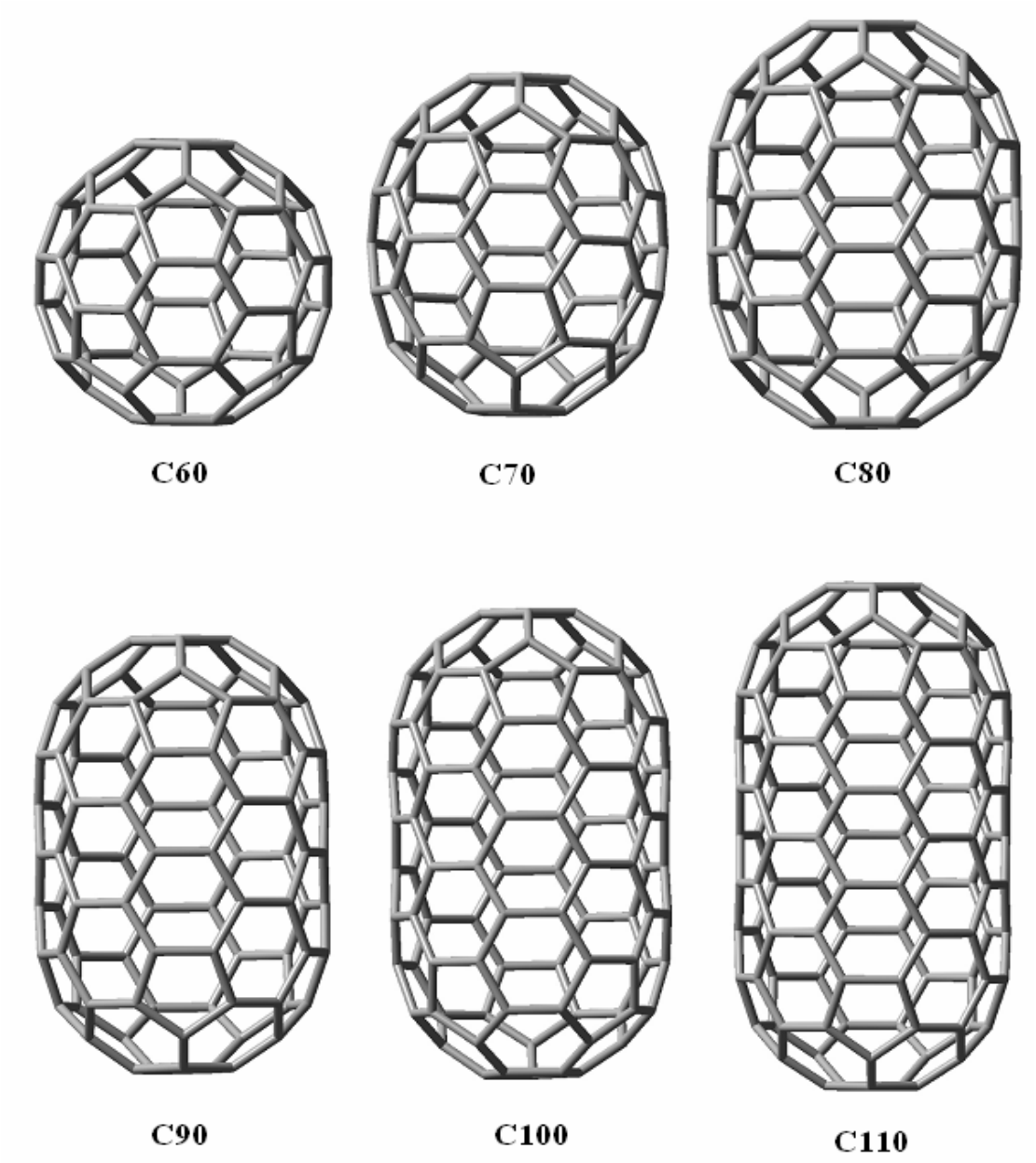

Figure 8 The series of [5,5]-single-walled carbon nanotubes capped with [60]-fullerene hemispheres.

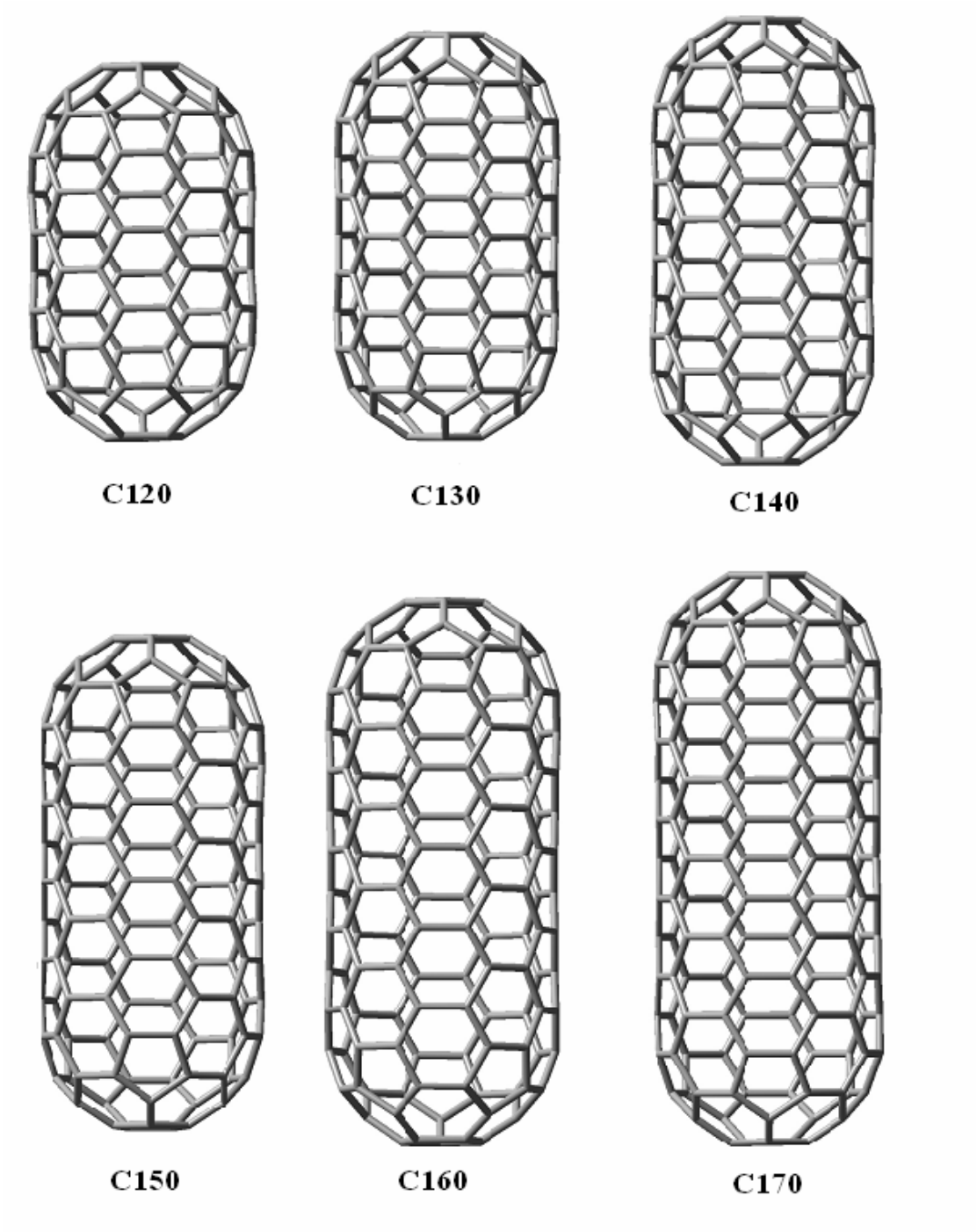

Figure 8 (Cont'd)

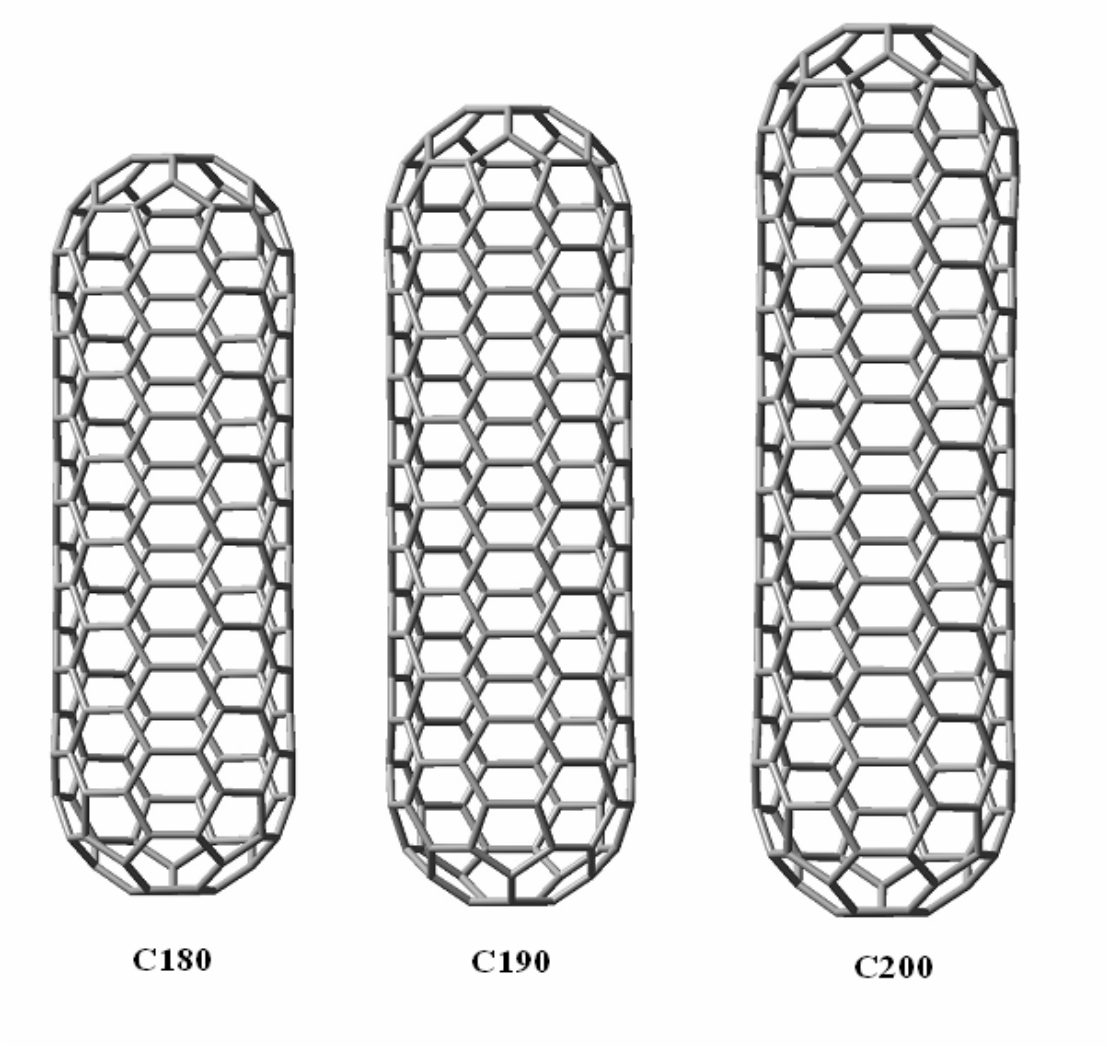

Figure 8 (Cont'd)

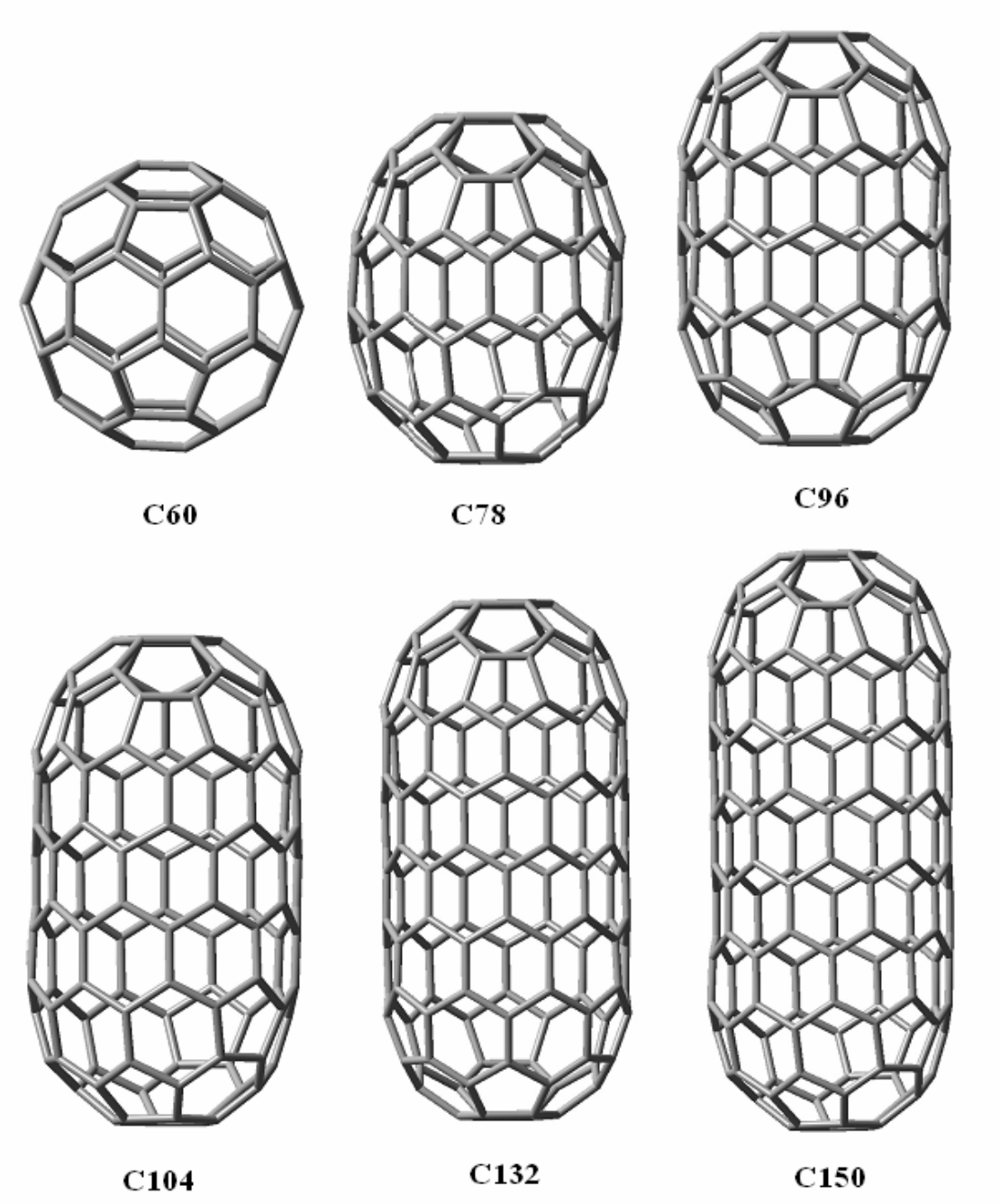

Figure 9 The series of [9,0]-single-walled carbon nanotubes capped with [60]-fullerene hemispheres.

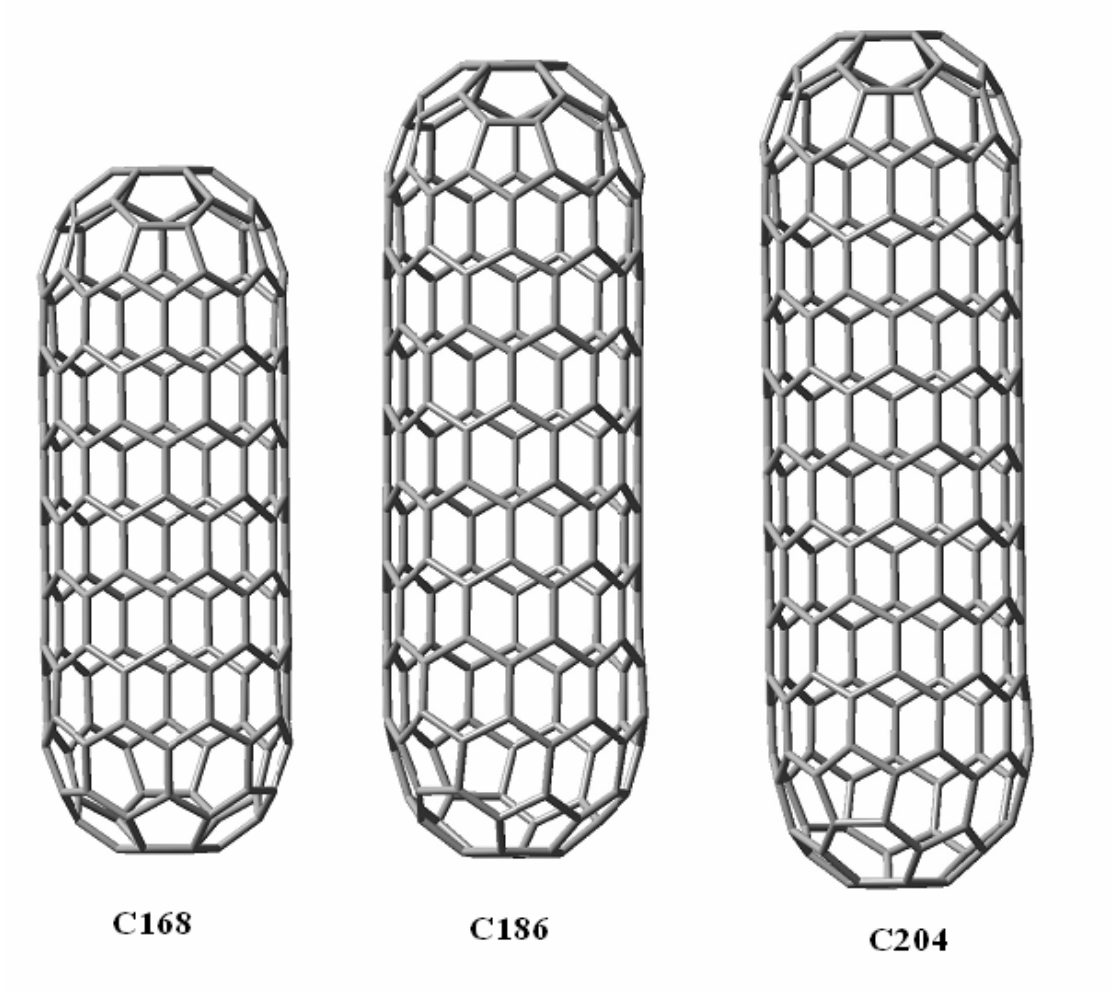

Figure 9 (Cont'd)

RESULTS AND DISCUSSIONS

1. Geometrical features of [60]-fullerene and carbon nanotubes

"Carbon nanotubes are originally the derivatives of fullerene" said Prof. Richard E. Smalley (Collins *et al.,* 1997). Two possible SWNTs capped with [60]-fullerene hemispheres consist of the [5,5] armchair nanotubes with a C_5 rotation axis and the [9,0] zigzag nanotubes with a C_3 rotation axis. The [60]-fullerene can be partitioned into a haft cyclic *cis*-polyene chain with 10 carbon atoms and two corrannulene-like caps along the C_5 rotation axis, and it can also be viewed as one *trans*-polyene chain with 18 carbon atoms and two sumanene-like caps along the C_3 rotation axis.

1.1 Geometrical features of [60]-fullerene

We first fully optimized the structure of [60]-fullerene with I_h symmetry using the PBE/def-SV(P) method implemented in the TURBOMOLE program package. Figure 10a shows the optimized [60]-fullerene I_h structure, where the 5–6 and 6–6 bonds are 1.453 and 1.390 Å, respectively. These values agree well with 1.459 and 1.398 Å of the 5–6 and 6–6 bonds, respectively obtained by using the B3LYP/6-31G(d) level of theory. Furthermore, these values still agree well with those obtained from a neutron diffraction experiment (David *et al.,* 1991). Additionally, these values have implied that the PBE/def-SV(P) approach can predict the effect of the length and type of SWNTs on the 1,3-dipolar cycloaddition onto their cap end. This is because we cannot employ more expensive methods to calculate a big system, in some cases consisting of over 4,000 basis functions.

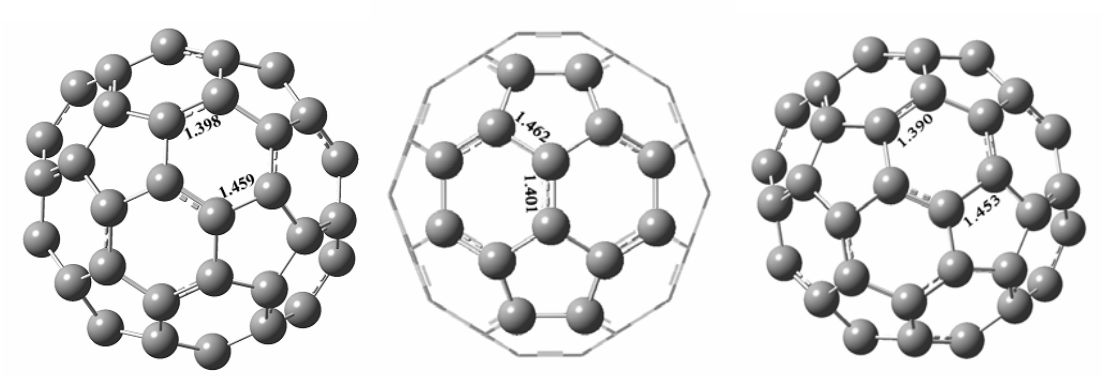

(a) (b) (c)

Figure 10 (a) The B3LYP/6-31G(d) optimized [60]-fullerene structure.
(b)The ONIOM(B3LYP/6-31G(d):AM1) optimized [60]-fullerene structure.
(c) The PBE/def-SV(P) optimized [60]-fullerene I_h structure.

Simultaneously, we have compared such methods with the popular hybrid ONIOM(B3LYP/6-31G(d):AM1) approach used by a number of computational chemists (Lu *et al.,* 2002; 2003; Warakulwit *et al.,* 2005). The 5-6 and 6-6 bonds obtained by using this ONIOM2 level are equal to 1.462 and 1.401 Å, respectively (cf. Figure 10b). These bonds are elongated in comparison with the corresponding values (1.459 Å vs. 1.398 Å and 1.453 Å vs. 1.390 Å) derived by the B3LYP/6-31G(d) and PBE/def-SV(P) methods, respectively (cf. Figure 10a and 10c). This shows that the combination between B3LYP and AM1 methods might not give the accurate geometrical features of [60]-fullerene derivatives, [5,5] armchair and [9,0] zigzag carbon nanotubes capped with [60]-fullerene hemispheres.

1.2 Geometrical features of the [5,5]-armchair single-walled carbon nanotubes capped with [60]-fullerene hemispheres

In this work, we obtained the optimized structures of a series of the [5,5]-armchair SWNTs caped with [60]-fullerene hemispheres (C_{40+20n}) using well-calibrated PBE/def-SV(P) method by starting with the smallest model, C_{70} where n = 1.5 up to the biggest model, C_{200} where n = 8.0. From this we found that the structure and the local aromaticity periodically fluctuate to generate three different structures: (1) a Kekule' network shown in Figure 11a which infers a 1,3,5-cyclohexatriene cyclic conjugate system; (2) a *p*-phenylene network flanked by peripheral double bonds is denoted as an incomplete Clar network (cf. Figure 11b); (3) an array of *p*-phenylene network that covers the whole tube structure, which is called a complete Clar network (cf. Figure 11c). Additionally, the Clar structure represents a benzene structure with equivalent C-C bond lengths.

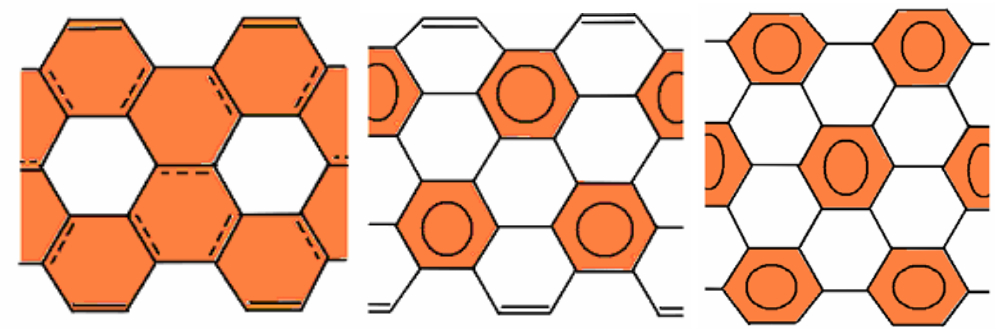

(a) (b) (c)

Figure 11 Three different structures of the [5,5]-SWNTs capped with [60]-fullerene hemispheres. (a) a Kekule' network. (b) an incomplete Clar network. (c) a complete Clar network.

Also, we have monitored the C-C bond length of a six-membered ring in the cyclic *cis*-polyene chain, and we then found that when the armchair nanotube is elongated layer-by-layer of 10 carbon atoms, the Kekule' networks

existed in the case of C_{70}, C_{100}, C_{130}, C_{160}, and C_{190} molecules shown in Figure 12, the incomplete Clar networks existed in the cases of C_{80}, C_{110}, C_{140}, C_{170}, and C_{200} molecules, and finally the complete Clar networks existed in the group of C_{90}, C_{120}, C_{150}, and C_{180} molecules. This agrees well with the previous work of Matsuo *el al.*, in 2003.

Furthermore, if we focus on the Kekule' structure of C_{70} shown in the first picture on the left of Figure 12, it will be found that the four C-C bond lengths monitored are 1.401 Å, 1.429 Å, 1.444 Å, and 1.452 Å, which is in good agreement with the 1.378 Å, 1.426 Å, 1.447 Å, and 1.462 Å of the information on an available X-ray. We can thus regard C_{70} as the first shortest armchair nanotubes and note that C_{70}, from which we created the C_{50}-hoop conjugation, consists only of the two10-carbon half-spheres and contains no structural features of armchair nanotubes. In addition, other molecules shown in Figure 12 will have the geometrical features like those of the Kekule's C_{70}. This is because we can not draw the Clar structure any more and are left with the Kekule's arrays. The further addition of 10 carbon atoms afforded C_{80} that comprises a row of incomplete Clar network. In the incomplete Clar structure of C_{40+20n}, where n = 2.0, 3.5, 5.0, 6.5, and 8.0 is shown in Figure 13, all bonds in the aromatic rings are about 1.43 Å of the C-C bond in a six-membered ring. Also, the one row of isolated olefins in the two edges flanking the Clar structure in the center is found. This indicates that this group has more of an aromatic feature than the previous group shown in Figure 12. In the next series, C_{90} has three rows of Clar array. The observed structural oscillation arises because of the match/mismatch array of the Clar benzene structure and one-dimensionality of CNTs: We can draw as many Clar structures as possible in the series C_{40+20n} where n = 2.5, 4.0, 5.5, and 7.0 (cf. Figure 14). Thus, we might expect that their absolute chemical hardness and HOMO-LUMO gap are sensitive to their length width like their geometry-optimized features.

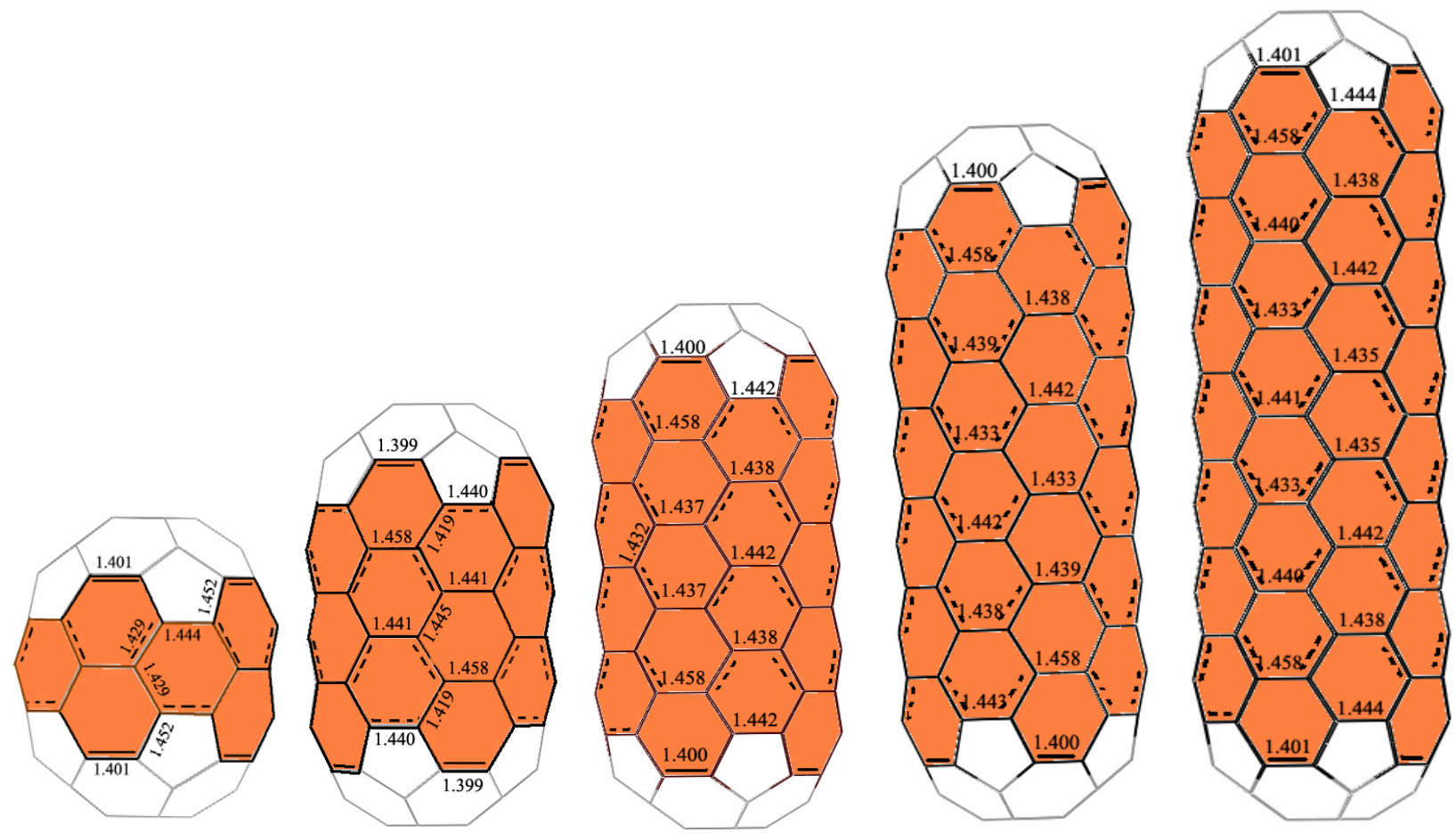

(C_{70}) (C_{100}) (C_{130}) (C_{160}) (C_{190})

Figure 12 The PBE/def-SV(P) optimized Kekule' structures of C_{40+20n} where n = 1.5, 3.0, 4.5, 6.0, and 7.5.

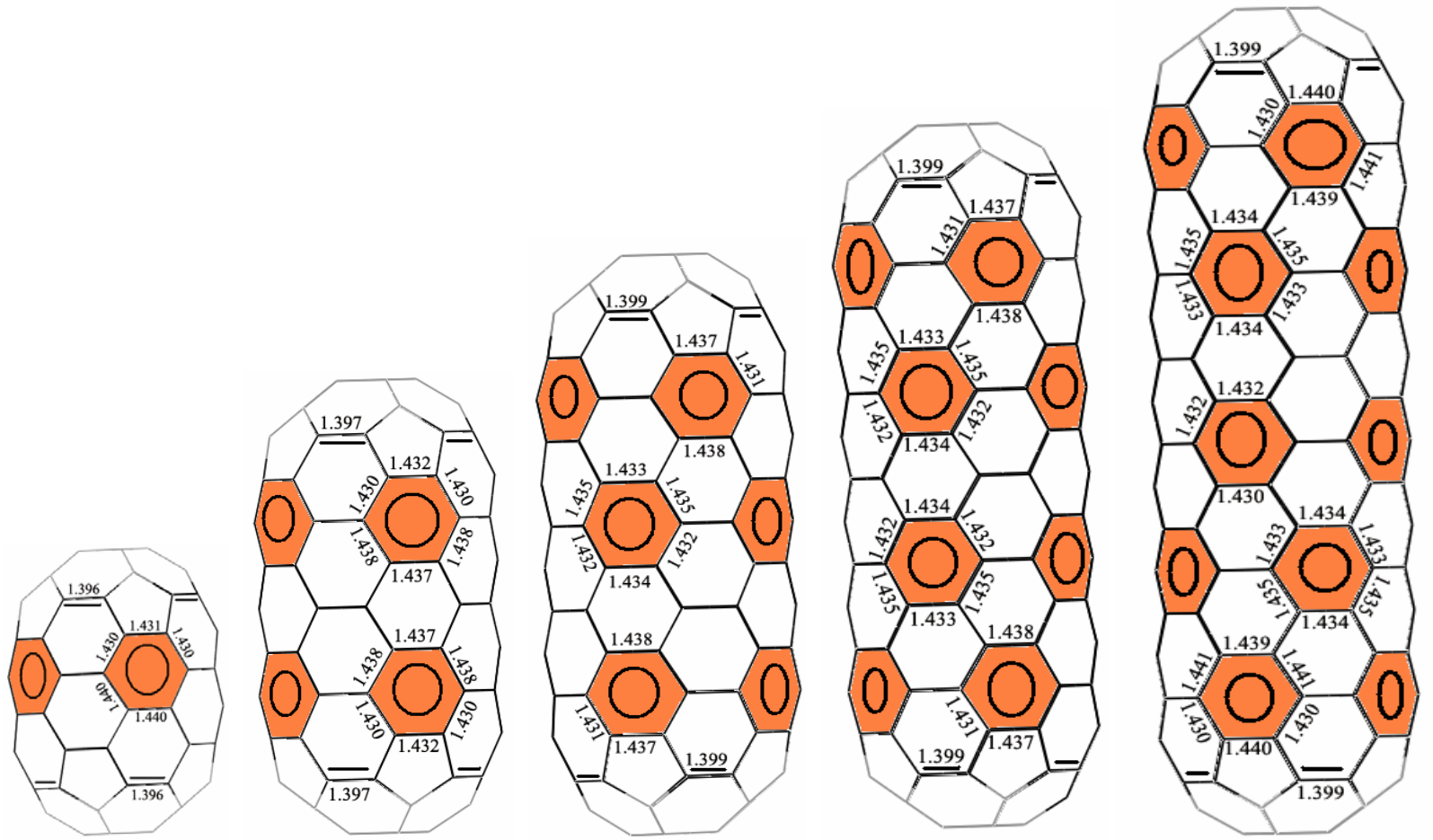

(C_{80}) (C_{110}) (C_{140}) (C_{170}) (C_{200})

Figure 13 The PBE/def-SV(P) optimized incomplete Clar structures of C_{40+20n} where n = 2.0, 3.5, 5.0, 6.5, and 8.0.

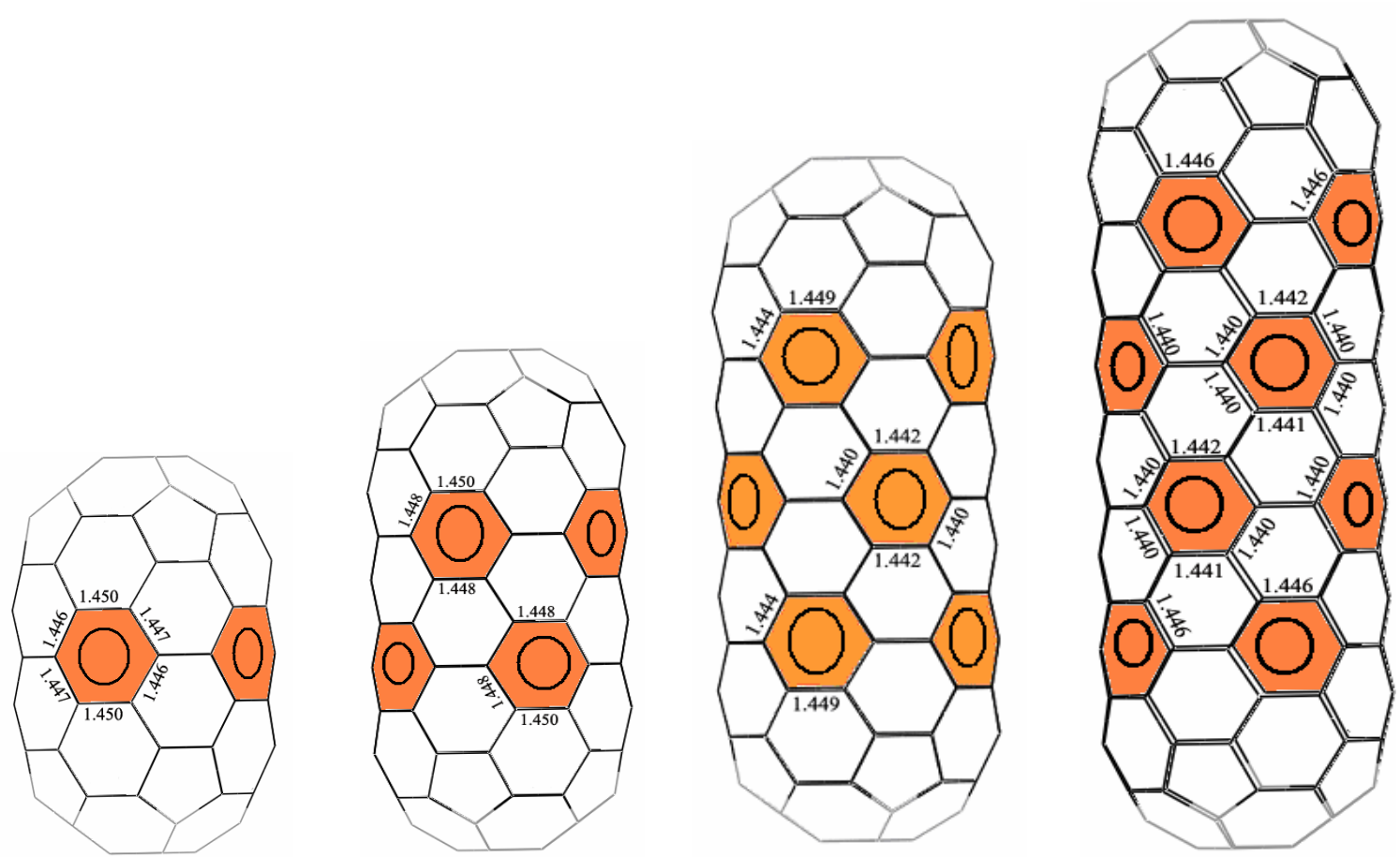

(C_{90}) (C_{120}) (C_{150}) (C_{180})

Figure 14 The PBE/def-SV(P) optimized complete Clar structures of C_{40+20n} where n = 2.5, 4.0, 5.5, and 7.0.

1.3 Geometrical features of the [9,0]-zigzag single-walled carbon nanotubes capped with [60]-fullerene hemispheres

In contrast to the armchair series, the optimized bond length of cyclic *trans*-polyene chain structures in the zigzag series do not sensitively depend on the cylinder bond length. The similar C-C bond lengths in a six-membered ring do not exist in the zigzag series shown in Figure 15. For example, in the case of C_{78} molecule, there are three different C-C bond lengths (1.432 Å, 1.455 Å, and 1.472 Å) in such a ring. Also, when the number of cyclic *trans*-polyene increases the distinct type of C=C bond (one being shorter than 1.42 Å) exists, such as 1.388 Å for C_{96} and C_{114}, 1.391 Å for C_{132} and C_{150}, as well as 1.392 for C_{168}). These are the characteristics of the Kekule' network structure because we cannot draw anymore Clar structures and are left with the Kekule' arrays. As a result, we might expect that their absolute chemical hardness and HOMO-LUMO gap are insensitive to their length width like their geometry-optimized features.

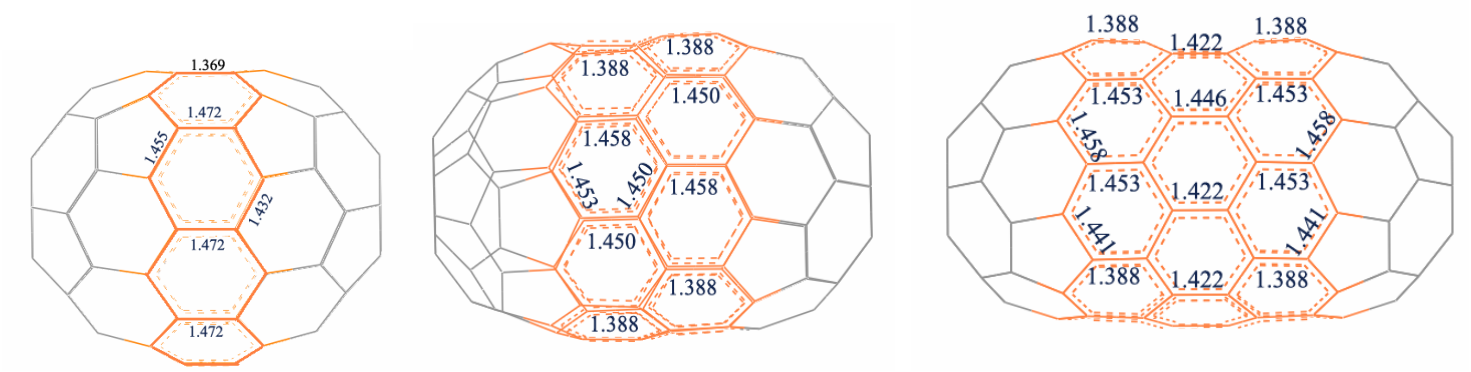

(C_{78}) (C_{96}) (C_{114})

(C_{132}) (C_{150})

Figure 15 The PBE/def-SV(P) optimized Kekule's structures of a series [9,0] zigzag SWNTs capped with hemispheres of [60]-fullerene.

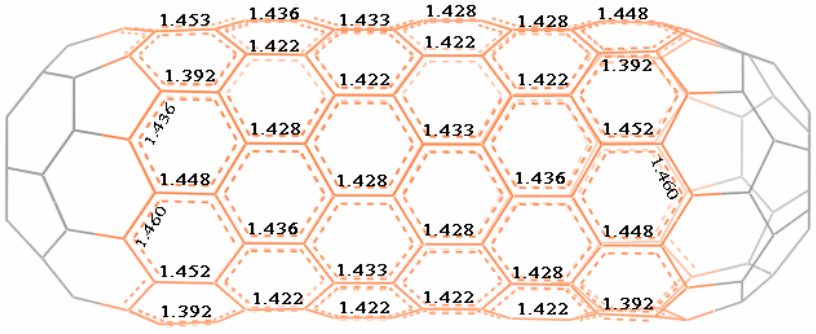

(C_{168})

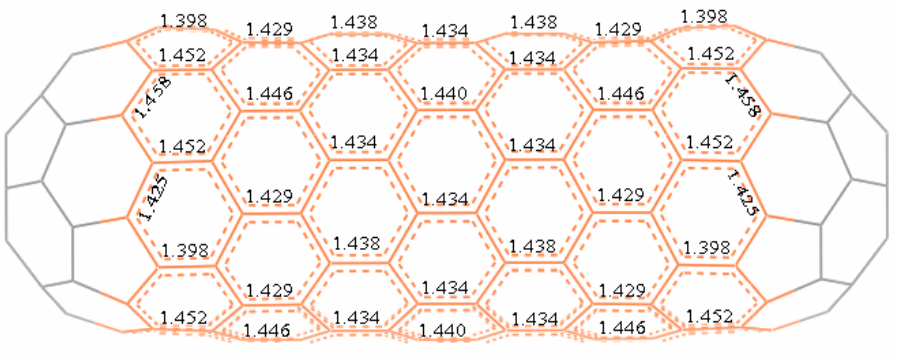

(C_{184})

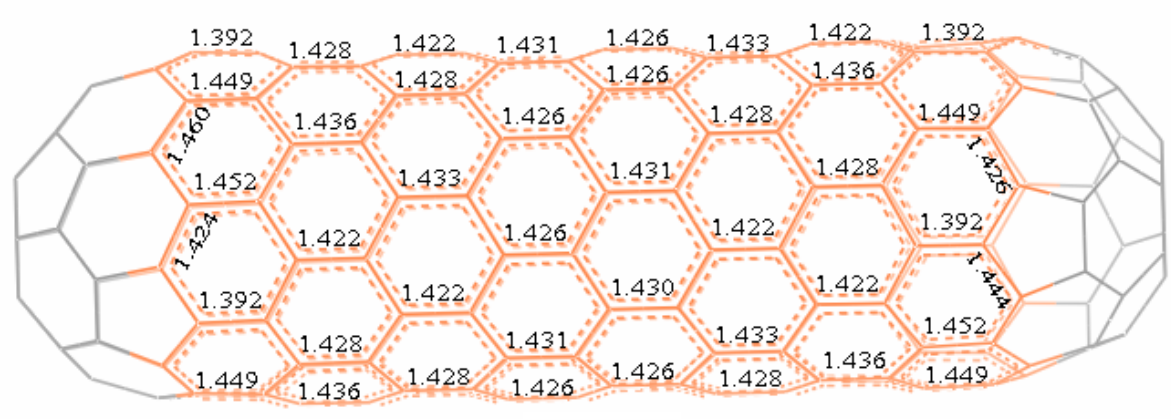

(C_{204})

Figure 15 (Con't)

2. Effect of the number of *cis*- and *trans*-cyclic polyene units on reactivity trends

The trends in the chemical potential energy barriers of the 1,3-dipolar cycloaddition of ozone onto the fullerene hemisphere of the two series of the capped [5,5]-armchair and [9,0]-zigzag single-walled carbon nanotubes can be correlated with the useful reactivity indices, chemical hardness, **η**, and the Frontier Molecular Orbital (FMO) interaction between nanotubes and ozone. These indices are theoretically based on the electronic structure of the frontier molecular orbital of reactants (Buhl *et. al.* 2001). Noted, however, is that while increasing the number of cyclic polyene units, only 14 carbon atoms shown in Figure 7a are computed at the high level of theory (B3LYP/6-31G(d)) while the rest are evaluated at the low level of theory (AM1). Although this region might not be big enough to describe the electronic properties of the whole [60]-fullerene and nanotube materials, to study the local reactivity of a particular site, it has been proven to provide quite reliable results in predicting the reactivity trend of the 1,3-dipolar cycloaddition reaction of ozone onto the sidewall of open-ended nanotubes (Lu *et al.,* 2003). By using the ONIOM method, the influence of the environment, computed at a low level of theory, on the electronic properties of the high level shell is indirectly taken into account mechanically. Therefore, increasing the number of cyclic polyene units in the low level shell of carbon nanotubes would have, to some extent, an effect on the molecular electronic properties of the high level part. On the other hand, these properties can be elucidated by using the full density functional theory called PBE method. It is appropriate not only for predicting the reactivity trend of high-symmetry but also for analyzing the effect of the CNT length to the 1,3- dipolar cycloaddition of ozone on the cap of two series of [5,5] armchair and [9,0] zigzag single-walled carbon nanotubes capped with fullerene hemispheres.

2.1. Chemical hardness (η)

Chemical hardness is the reactivity index that relates to the resistance to change in the electron number or deformation of the electron cloud in molecules. Thus, the molecules or materials that exhibit high reactivity correlate with the small values of their chemical hardness (Lee *et al.,* 1988; Parr *et al.,* 1983; Zhou *et al.,* 1988; Buhl *et al.,* 2001). Within the density functional theory (DFT) formalism, the chemical hardness, **η**, is defined as

$$\eta = (\text{HOMO-LUMO})/2 \qquad (4)$$

where HOMO is the Highest Occupied Molecular Orbital energy and LUMO is the Lowest Unoccupied Molecular Orbital energy.

As listed in Table 1, the HOMO and LUMO energies of [60]-fullerene are calculated to be -5.99 and -3.17 eV at the ONIOM(B3LYP/6-31G(d):AM1) technique, corresponding to the energy gap (HOMO-LUMO) of 2.82 eV, which slightly overestimates the result derived from full optimization at the B3LYP/6-31G(d) level of theory of 2.75 eV (Yumura *et al.,* 2004). Nevertheless, the corresponding values are equal to -5.81 and -4.16 eV, respectively at the PBE method, as a result the energy gap of 1.65 eV that significantly underestimates this benchmark.

The chemical hardness (**η)** of [60]-fullerene computed from Equation (4) of 0.82 eV at the PBE level of theory are virtually higher than this, which are obtained from the [9,0]-zigzag nanotubes series, shown in the dash line of Figure 16. The **η** of these materials slightly decrease from the number of *trans*-polyene chain (n) of 1.0 to 4.0 and after that it is stable at about 0.3 eV. Whereas, the **η** of [5,5] nanotubes series, shown in the solid line of Figure 16, periodically fluctuates from 0.85 eV at the n of 1.5 to 0.15 eV at

the n of 8.0. This is because, in the case of armchair nanotubes, there are three different classes, which are referred to as; (1) a Kekule´ network, in the case that n are 1.5, 3.0, 4.5, 6.0, and 7.5, (2) an incomplete Clar network, where n are 2.0, 3.5, 5.0, 6.5, and 8.0, and (3) a complete Clar network, where n are 1.0, 2.5, 4.0, 5.5, and 7.0. This is, in addition, agreeable with the previous information of Matsuo *et al.*, (2003).

From these results, we might expect a higher reactivity for the 1,3-dipolar cycloaddition of ozone onto the hemisphere of the two series of capped armchair and zigzag nanotubes than onto [60]-fullerene. Furthermore, the **η** value of the 14C (cluster) of [60]-fullerene at the ONIOM (B3LYP/6-31G (d):AM1) method is computed to be 0.52 eV, not corresponding to the **η** of 1.38 eV, which is fully optimized at B3LYP/6-31G(d) (Cioslowski *et al.*, 2002; Yumura *et al.,* 2004). Moreover, the relationship between **η** and the number of cyclic polyene units, n, in the two series of the finite-length nanotubes, shown in Figure 16, have still indicated that, in the case of PBE calculations, the increasing chain length has a significant effect on both electronic properties and geometries of the active center but, in the case of ONIOM(B3LYP/6-31G(d):AM1), it does not have a considerable effect since the **η** is stable at about 0.5 eV for both nanotubes, which disagrees to the probably accurate value, carried out at B3LYP/6-31G(d) (Cioslowski *et al.,* 2002). These have implied that the 14C (cluster) at the high level of theory is inadequate for predicting the electronic properties of nanotubes. To confirm this statement, the critical C1-C2 bond length of all nanotubes, shown in Figure 17, has been considered as well. Accordingly, we have found that it does not significantly change in the case of the ONIOM (B3LYP/6-31G(d):AM1). The C1-C2 bond length of nanotubes is at about 1.40 Å; hence, the increasing number of cyclic polyene units does not lower the energy gap between the HOMO and LUMO orbitals. This is due to the use of a small active model in the high level layer,

which is not quantitatively able to reproduce the molecular electronic properties of the entire materials. Nevertheless, the agreement of lowering the energy gap with increasing chain length is found in the low level of theory.

Not only has the effect of the CNT length been scrutinized but the effect of symmetry point groups of nanotubes has been considered as well. From Figure 18, the HOMO-LUMO gap of D_{5h}-armchair nanotubes dramatically decreases from 1.62 eV to 0.4 eV in the case that the number of *cis*-polyene chain (n) alters from 1 to 5. After that, it goes up 1.20 eV when n is 7. Subsequently, it slowly stabilizes when n increases. Simultaneously, the effect of D_{5d} point group to armchair nanotubes is alike that of the D_{5h} point group.

In the case of zigzag nanotubes (Figure 19), if the number of *trans*-polyene (n) increase, then the HOMO-LUMO gap will slightly decrease. Also, it will be stable when n is after 6 for all point groups. However, when we have compared the energy gap to different symmetries, we would find that the D_3-zigzag nanotubes have a more narrow energy gap than the D_{3d}- and D_{3h}-zigzag nanotubes, respectively.

Table 1 The HOMO, LUMO, and η of [60]-fullerene and two series [5,5]-armchair and [9,0]- zigzag single-wall carbon nanotubes capped with fullerene hemisphere.

Species (Symmetry)	HOMO (eV)			LUMO (eV)			η (eV)		
	SP[a]	14C[b]	PBE[c]	SP[a]	14C[b]	PBE[c]	SP[a]	14C[b]	PBE[c]
C_{60} (I_h)	-5.99	-2.50	-5.81	-3.17	-1.46	-4.16	1.41	0.52	0.83
[5,5] Armchair SWNTs									
C_{70} (D_{5h})	-5.92	-2.52	-5.81	-3.18	-1.41	-4.12	1.37	0.55	0.85
C_{80} (D_{5d})	-4.89	-2.46	-4.99	-3.93	-1.47	-4.64	0.48	0.49	0.18
C_{90} (D_{5h})	-5.31	-2.49	-5.23	-3.29	-1.44	-4.22	1.01	0.52	0.51
C_{100} (D_{5d})	-5.48	-2.51	-5.44	-3.14	-1.43	-4.07	1.17	0.54	0.69
C_{110} (D_{5h})	-4.61	-2.47	-4.89	-3.92	-1.46	-4.49	0.34	0.50	0.20
C_{120} (D_{5d})	-4.96	-2.49	-4.96	-3.44	-1.45	-4.31	0.76	0.52	0.33
C_{130} (D_{5h})	-5.20	-2.50	-5.19	-3.21	-1.43	-4.11	0.99	0.53	0.54
C_{140} (D_{5d})	-4.46	-2.48	-4.81	-3.91	-1.46	-4.42	0.28	0.51	0.20
C_{150} (D_{5h})	-4.76	-2.49	-4.81	-3.53	-1.45	-4.36	0.61	0.52	0.22
C_{160} (D_{5d})	-4.98	-2.50	-5.00	-3.26	-1.44	-4.13	0.86	0.53	0.44
C_{170} (D_{5h})	-4.52	-2.51	-4.77	-3.92	-1.43	-4.38	0.30	0.54	0.20
C_{180} (D_{5d})	-4.62	-2.49	-4.74	-3.59	-1.45	-4.35	0.51	0.52	0.20
C_{190} (D_{5h})	-4.82	-2.50	-4.88	-3.35	-1.44	-4.18	0.74	0.53	0.35
C_{200} (D_{5d})	-4.50	-2.50	-4.71	-3.87	-1.43	-4.40	0.32	0.54	0.15

[a] SP is a single point at B3LYP/6-31G(d)//ONIOM(B3LYP/6-31G(d):AM1)

[b] 14C (cluster) at ONIOM(B3LYP/6-31G(d):AM1)

[c] PBE/def-SV(P)

Table 1 (Cont'd)

Species (Symmetry)	HOMO (eV)			LUMO (eV)			η (eV)		
	SP[a]	14C[b]	PBE[c]	SP[a]	14C[b]	PBE[c]	SP[a]	14C[b]	PBE[c]
[9,0] Zigzag SWNTs									
C_{78} (D_{3h})	-4.82	-2.49	-5.54	-3.35	-1.43	-4.11	0.74	0.53	0.72
C_{96} (D_{3d})	-5.47	-2.49	-5.35	-3.24	-1.43	-4.18	1.11	0.53	0.58
C_{114} (D_{3h})	-4.94	-2.49	-5.20	-3.61	-1.43	-4.15	0.66	0.53	0.53
C_{132} (D_{3d})	-5.11	-2.49	-5.08	-3.33	-1.43	-4.21	0.89	0.53	0.43
C_{150} (D_{3h})	-4.74	-2.49	-4.99	-3.62	-1.43	-4.20	0.56	0.53	0.40
C_{168} (D_{3d})	-4.90	-2.49	-4.92	-3.39	-1.43	-4.23	0.75	0.53	0.34
C_{186} (D_{3h})	-4.62	-2.49	-4.87	-3.63	-1.43	-4.23	0.50	0.53	0.32
C_{204} (D_{3d})	-4.57	-2.49	-4.82	-3.62	-1.43	-4.25	0.47	0.53	0.28

[a] SP is a single point at B3LYP/6-31G(d)//ONIOM(B3LYP/6-31G(d):AM1)

[b] 14C (cluster) at ONIOM(B3LYP/6-31G(d):AM1)

[c] PBE/def-SV(P)

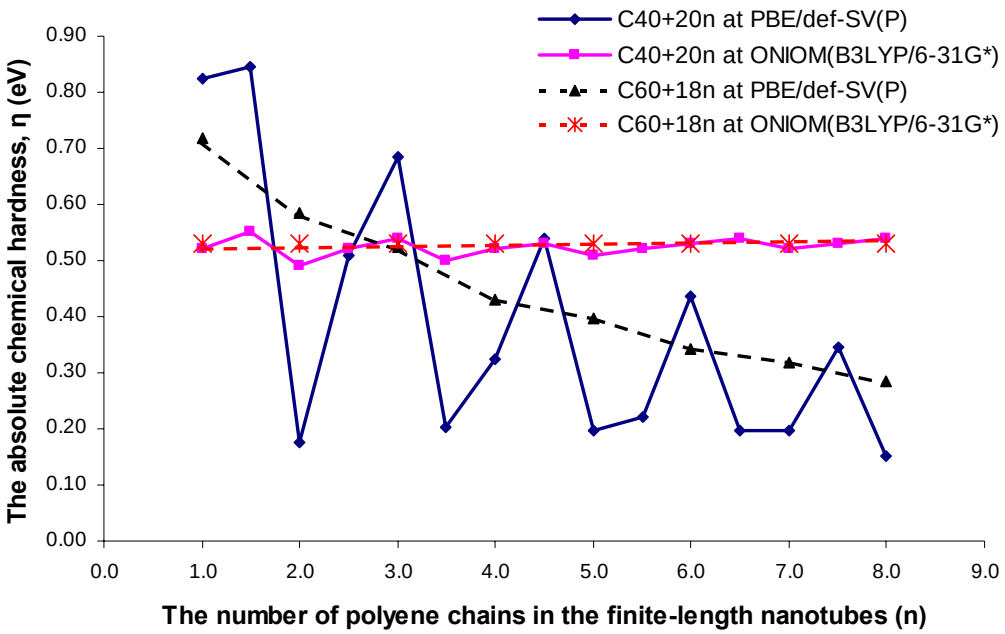

Figure 16 The absolute chemical hardness (η) of [60]-fullerene and nanotubes as a function of n.

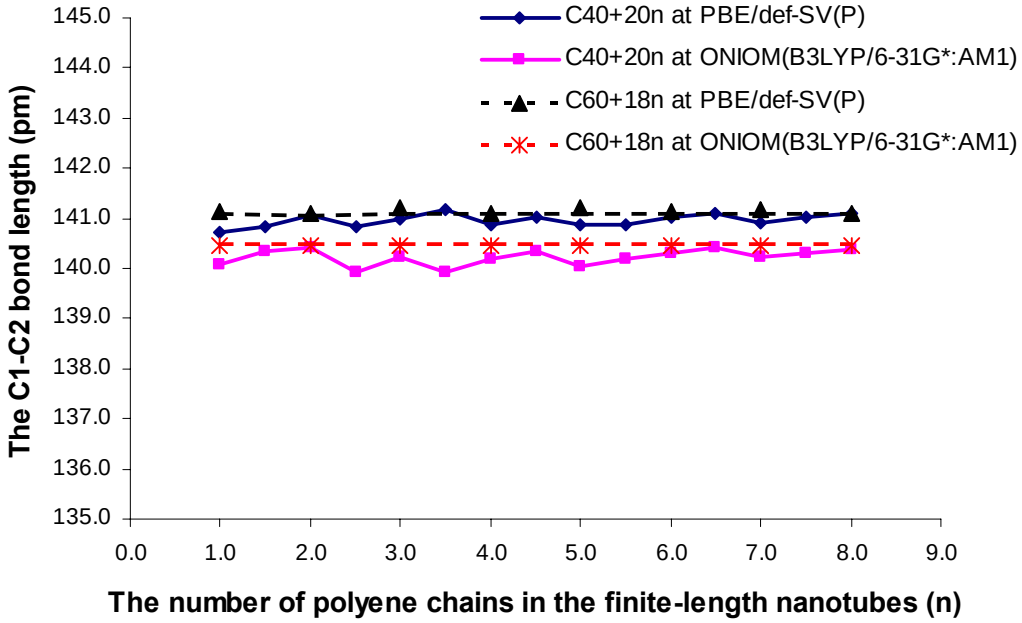

Figure 17 The critical C1-C2 bond length (pm) of [60]-fullerene and nanotubes as a function of n.

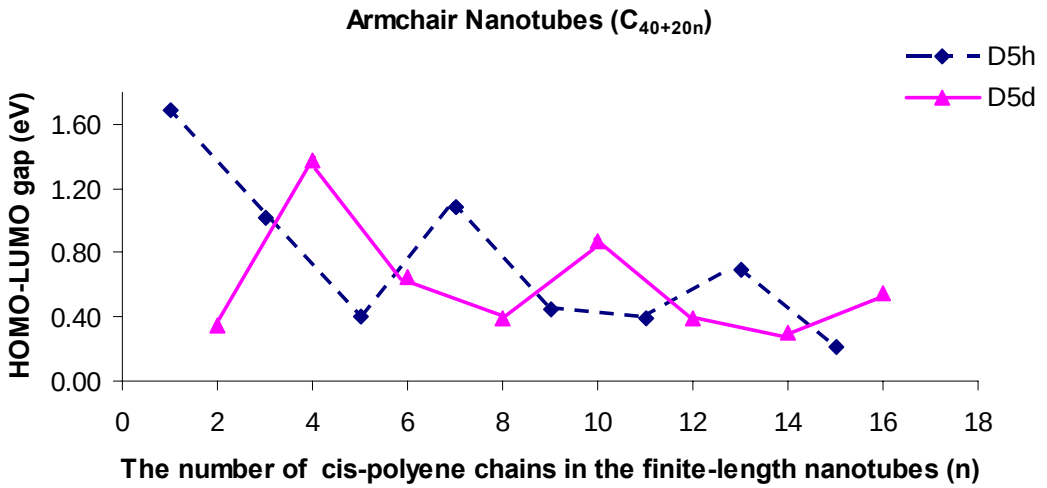

Figure 18 The effect of symmetry point group on the PBE/def-SV(P) calculated HOMO-LUMO gap of [5,5] Armchair nanotubes.

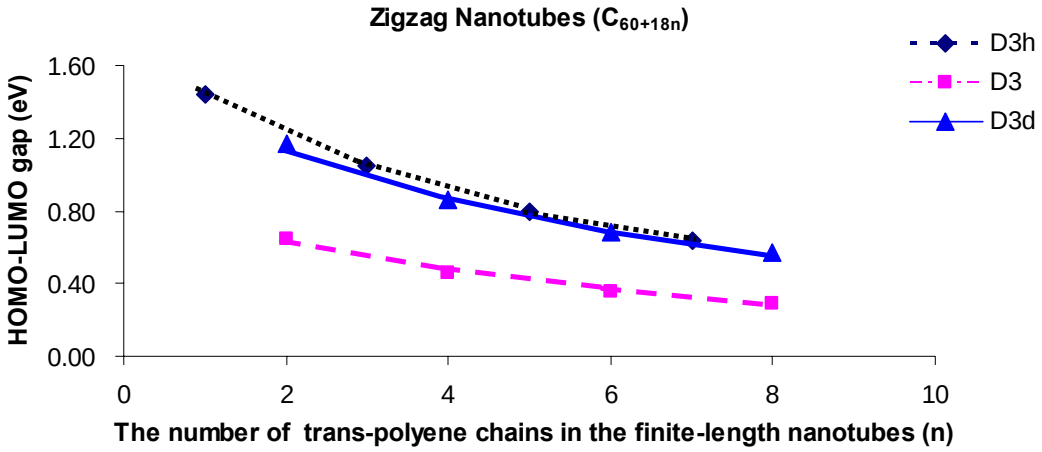

Figure 19 The effect of symmetry point group on the PBE/def-SV(P) calculated HOMO-LUMO gap of [9,0] Zigzag nanotubes.

2.2. Frontier molecular orbital (FMO) interaction

Frontier molecular orbital interaction is frequently used to predict the reactivity of the reaction between two molecular π-systems (Lu *et al.*, 2003). The 1,3-dipolar cycloaddition of ozone with nanotubes capped with fullerene hemisphere relies on the frontier molecular orbital interaction between dipolar (ozone) and dipolarphiles ([60]-fullerene and nanotubes). Two energy differences between the frontier molecular orbitals (LUMO and HOMO) of dipolar and dipolarphile can be calculated by the following equations:

$$\Delta E^{N} = E_{LUMO}(\text{ozone}) - E_{HOMO}(\text{nanotubes}) \quad (5)$$

$$\Delta E^{I} = E_{LUMO}(\text{nanotubes}) - E_{HOMO}(\text{ozone}) \quad (6)$$

where ΔE^{N} is a normal frontier molecular orbital interaction, ΔE^{I} is an inverse frontier molecular orbital interaction, E_{LUMO} is the Lowest Unoccupied Molecular Orbital energy, and E_{HOMO} is the Highest Occupied Molecular Orbital energy.

From the frontier molecular orbital theory, the smaller the molecular orbital (MO) energy differences between the dipolar and dipolarphile, the lower the activation energy (Lu *et al.*, 2003; Warakulwit *et al.*, 2004). In this study, the MO energy difference between the dipolar LUMO and dipolarphile HOMO is smaller than that between the dipolarphile LUMO and dipolar HOMO. Therefore, in the 1,3-cycloaddition reaction, ozone prefers to use its LUMO to interact with the HOMO of dipolarphile (Hendrickx *et al*., 2003), as shown in Figure 20.

Similar to the results obtained from the absolute chemical hardness, the characteristic of MO energy interaction of the ozone LUMO and nanotube

HOMO, calculated using the PBE/def-SV(P), fluctuates from 0.05 eV to -1.05 eV for the armchair series when n increases from 1.0 to 8.0. However, the formalism of fluctuation will depend on the three different classes of their structures-- Kekule', incomplete Clar, and complete Clar networks (Matsuo *et al*., 2003). Also, the PBE/def-SV(P) calculated FMO energies of zigzag series will slightly decline from -0.22 eV to -0.94 eV with increasing the chain length (cf. Table 2 and Figure 21).

Moreover, from the MO energy interaction in Table 2, we can predict the two series of nanotubes in the 1,3-dipolar cycloaddition reaction have a higher reactivity on than [60]-fullerene. The energy differences between the ozone LUMO and HOMO of the [60]-fullerene is calculated is 0.05 eV but this, as of most, [5,5]-armchair and [9,0]-zigzag series are calculated to be lower. Again, the ONIOM results, shown in Table 2 and Figure 21, have indicated that this method can not predict the trend of FMO interactions of ozone and nanocarbons. This is because they are superior conducting materials (Tang *et al.,* 2001); therefore, the effect of a low model is needed to ensure the free movement of electron.

Table 2 The FMO interactions of ozone (dipolar) with the [60]-fullerene and two series [5,5]-armchair and [9,0]-zigzag single-walled carbon nanotubes capped with fullerene hemisphere (dipolarphile).

Species	ΔE^N (eV)			ΔE^I (eV)		
	SP[c]	14C[d]	PBE[f]	SP[c]	14C[d]	PBE[f]
C_{60} (I_h)	0.97	-0.02	0.05	5.94	3.10	3.27
C_{70} (D_{5h})	0.90	0.01	0.05	5.94	3.14	3.31
C_{80} (D_{5d})	-0.13	-0.06	-0.77	5.19	3.09	2.79
C_{90} (D_{5h})	0.29	-0.02	-0.53	5.82	3.11	3.21
C_{100} (D_{5d})	0.46	-0.01	-0.32	5.98	3.13	3.36
C_{110} (D_{5h})	-0.41	-0.04	-0.87	5.19	3.10	2.94
C_{120} (D_{5d})	-0.06	-0.02	-0.80	5.67	3.11	3.12
C_{130} (D_{5h})	0.18	-0.01	-0.58	5.91	3.13	3.32
C_{140} (D_{5d})	-0.56	-0.04	-0.95	5.21	3.10	3.01
C_{150} (D_{5h})	-0.27	-0.02	-0.95	5.58	3.11	3.07
C_{160} (D_{5d})	-0.04	-0.01	-0.76	5.86	3.12	3.30
C_{170} (D_{5h})	-0.50	-0.01	-0.99	5.20	3.13	3.05
C_{180} (D_{5d})	-0.40	-0.02	-1.02	5.52	3.11	3.08
C_{190} (D_{5h})	-0.20	-0.02	-0.88	5.77	3.12	3.25
C_{200} (D_{5d})	-0.52	-0.01	-1.05	5.25	3.13	3.03

$\Delta E^N = E_{LUMO}$(ozone) - E_{HOMO}(nanotubes)

$\Delta E^I = E_{LUMO}$ (nanotubes) - E_{HOMO} (ozone)

[c] SP is a single point at B3LYP/6-31G(d)//ONIOM(B3LYP/6-31G(d):AM1)

[d] 14C (cluster) at ONIOM(B3LYP/6-31G(d):AM1)

[e] PBE/def-SV(P)

Table 2 (Cont'd)

Species	ΔE^N (eV)			ΔE^I (eV)		
	SP[c]	14C[d]	PBE[f]	SP[c]	14C[d]	PBE[f]
C_{78} (D_{3h})	-0.20	-0.02	-0.22	5.77	3.13	3.32
C_{96} (D_{3d})	0.44	-0.02	-0.42	5.87	3.13	3.25
C_{114} (D_{3h})	-0.08	-0.02	-0.56	5.50	3.13	3.28
C_{132} (D_{3d})	0.09	-0.02	-0.68	5.78	3.13	3.22
C_{150} (D_{3h})	-0.28	-0.02	-0.77	5.50	3.13	3.23
C_{168} (D_{3d})	-0.13	-0.02	-0.84	5.73	3.13	3.20
C_{186} (D_{3h})	-0.41	-0.02	-0.89	5.49	3.13	3.20
C_{204} (D_{3d})	-0.45	-0.02	-0.94	5.49	3.13	3.18

$\Delta E^N = E_{LUMO}$(ozone) - E_{HOMO}(nanotubes)

$\Delta E^I = E_{LUMO}$ (nanotubes) - E_{HOMO} (ozone)

[c] SP is a single point at B3LYP/6-31G(d)//ONIOM(B3LYP/6-31G(d):AM1)

[d] 14C (cluster) at ONIOM(B3LYP/6-31G(d):AM1)

[e] PBE/def-SV(P)

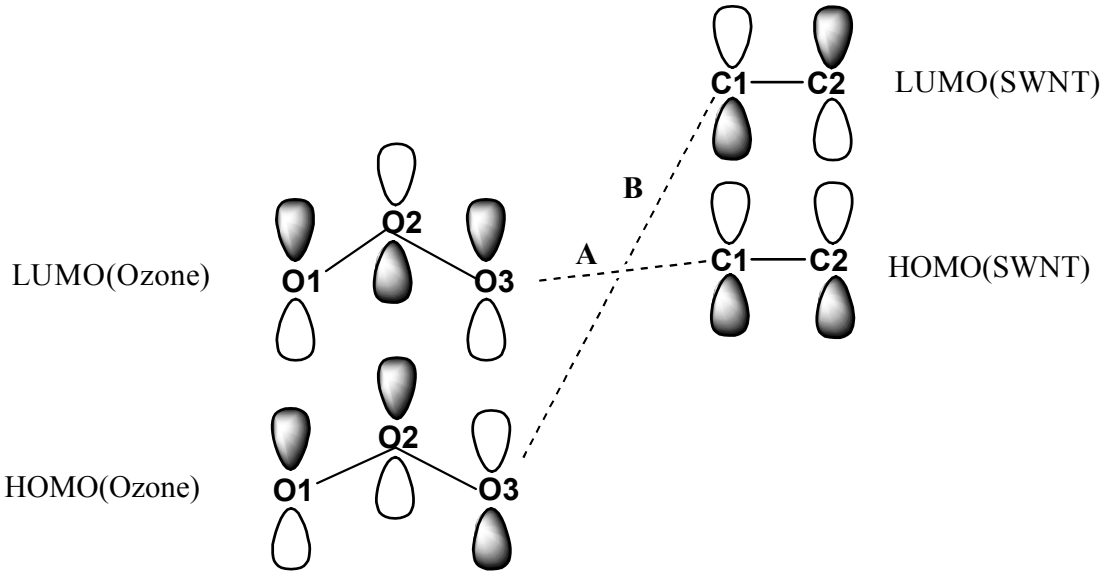

Figure 20 FMO interactions: A. leading to cycloadditions; B. not leading to cycloadditions.

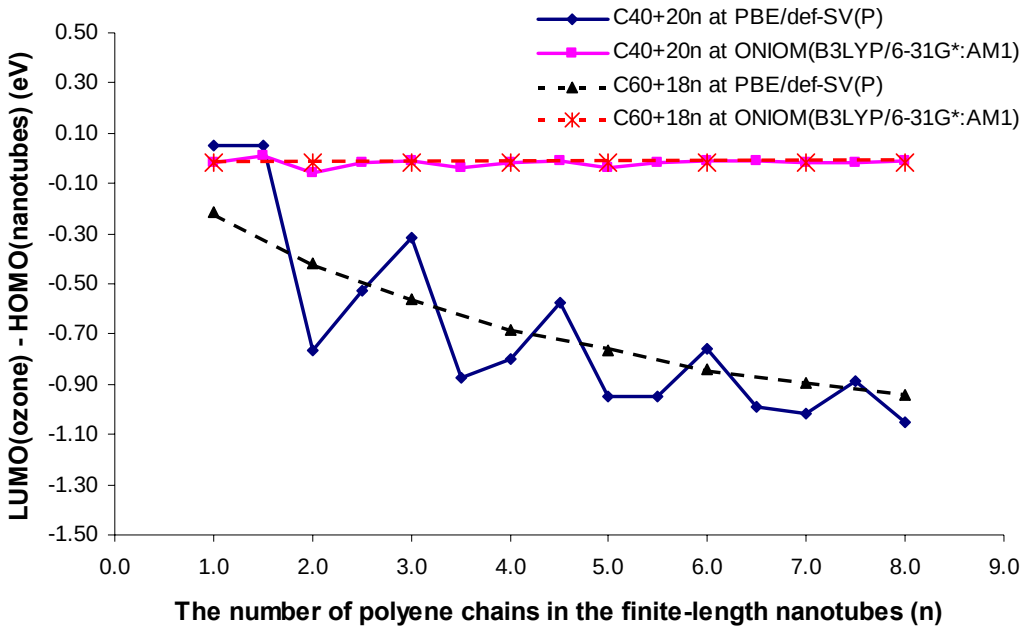

Figure 21 The interacted FMOs as a function of n.

3. The functionalization of [60]-fullerene and [5,5]-armchair and [9,0]-zigzag single-walled carbon nanotube capped with [60]-fullerene hemisphere

First, the quality of the ONIOM(B3LYP/6-31G(d):AM1) method has been tested by comparing the optimized geometrical parameters of reactants with available experimental observations. The calculated critical C1-C2 bond length, which is focused as the reaction site, is 1.401 Å, 1.402 Å, and 1.405 Å for [60]-fullerene, [5,5]-armchair, and [9,0]-zigzag nanotubes respectively. The first value is in excellent agreement with the value obtained from the electron diffraction method for [60]-fullerene of 1.401 Å (Hamada *et al.,* 1992). The calculated O-O bond distance (1.264 Å) and O-O-O bond angle (117.9^{o}) of ozone are comparable with the experimentally observed values (1.272 Å and 116.8^{o}) (Prakash *et al.,* 1980). Therefore, this method is still employed and expected to give reliable results for other geometrical parameters of intermediates along the reaction path. Selected optimized geometries of reactants, transition states (TS), and adducts (LM) are documented in Tables 3-4. For the energy barrier calculation, all transition state structures have been confirmed for the true saddle point, which possesses only one imaginary frequency, by the frequency calculation.

Together, although the ONIOM(B3LYP/6-31G(d):AM1) technique might not give the accurate number in the cases of the geometry and energy of adducts when it is compared with the full B3LYP theory, it can predict the useful trend of such properties, which will be useful when we are dealing with the big models. The basis functions in the biggest model are more than 4,000 functions. In this work, we have, therefore, employed the hybrid method (ONIOM2) to examine not only the effect of the type of SWNTs but the length of SWNTs as well on both chemisorption and activation energies. We have, in

addition, compared such properties with those obtained by means of PBE/def-SV(P).

3.1. The 1,3-dipolar cycloaddition of ozone onto [60]-fullerene

The study of 1,3-dipolar cycloaddition of ozone onto [60]-fullerene have started after we have tested the reaction mechanism of the ozonolysis of ethylene calculated by using B3LYP/6-31G(d,P). It appeared that the initial addition of O_3 to the double bond of the ethylene molecule is the most facile existing step of the overall oxidation process, like the 1,3-dipolar cycloaddition of ozone onto [60]-fullerene, illustrated in Figure 22, which follows a synchronous concerted pathway at the different levels of theory. In the transition state structure, the non-planar five-membered ring structure is formed. The O1 and O3 of ozone move toward the C1 and C2 of [60]-fullerene in an equivalent distance of 2.308 Å, 2.262 Å, and 2.302 Å for the B3LYP/6-31G(d), ONIOM(B3LYP/6-31G(d,p), and PBE/def-SV(P) levels of theory, respectively, resulting in the elongation of the C1-C2 bond to 1.426 Å, 1.438 Å, and 1.421 Å (cf. Figure 22). The predicted activation energy (E_a) is found to be 2.75, -1.02, 2.78, and -4.93 kcal/mol for the B3LYP/6-31G(d), ONIOM(B3LYP/6-31G(d,p):AM1), BSSE corrected at B3LYP/6-31G(d,p), and PBE/def-SV(P) levels of theory, respectively. It is found that the B3LYP and BSSE corrected E_a is only comparable with the experimental estimate of 2.5 kcal/mol for 2-*trans*-butene (Prakash *et al.,* 1980). The [60]-fullerene ozone adduct is immediately formed at the reactive center with the same conformation in the transition state structure (cf. Figure 23). The single bonds are formed between the O1 and O3 of ozone and the C1 and C2 of [60]-fullerene with the equal bond length of 1.439 Å, 1.432 Å, 1.431 Å, for such different methods. The C1-C2 bond is elongated to the value of 1.610 Å, 1.648 Å, and 1.605 Å. The chemisorption energy, with respect to the reactants, is calculated to be -46.09 kcal/mol for the B3LYP theory, -46.10 kcal/mol for the

ONIOM2 scheme and -37.83 kcal/mol for the PBE approach, which are less exothermic than in the case of 2-*trans*-butene of -54.5 kcal/mol (Prakash *et al.*, 1980). It is to note that the activation and chemisorption energies estimated by the ONIOM2 scheme are 2.78 and -46.26 kcal/mol, respectively. These are approximately the same value of -46.09 kcal/mol at the full B3LYP/6-31G(d) calculation. This is because the [60]-fullerene surface or the cap ends of nanotubes have lost the aromatization property. It has in addition been confirmed with the nucleus-independent chemical shift (NICS) analysis. The NICS(1) of six- and five-membered rings of [60]-fullerene surface are equal to 2.27 ppm and -0.33 ppm that lead to the C1-C2 bond, shown in Figure 7a, more reactive than C1-C3 bond, shown in Figure 7a. For the same reason, the NICS(1) of cap ends and side wall of SWNTs are nearly -0.34 ppm and -12.30 ppm (Matsuo *et al*., 2003). This shows that the sidewall of nanotube has more aromaticity than the cap ends of nanotube, which leads to that the side wall being more stable than the cap end as well.

Accordingly, it confirms the validation of the ONIOM method in predicting the energetic pathway. Since the [60]-fullerene is the prototype structure of the capped nanotubes, the 1,3-dipolar cycloaddition of ozone onto the fullerene hemisphere of the capped nanotubes should therefore display a similar manner as discussed above.

Simultaneously, if we center on the apparent activation energy (E_a) and chemisorption energy (E_r) in the different techniques, we will find that the both values of the B3LYP/6-31G(d)//ONIOM(B3LYP/6-31G(d):AM1) method closes to the those of the quantum mechanic method (B3LYP/6-31G(d)) more than the density functional approach (PBE/def-SV(P)). Activation energies are equal to -1.02 and -4.93 kcal/mol for the ONIOM(B3LYP/6-31G(d):AM1) and the PBE/def-SV(P) approaches, respectively. This shows that the 1,3-dipolar cycloaddition of ozone onto the surface of [60]-fullerene is facile. Although,

both methods might not be able to predict the exact values they are, nonetheless, able to be utilized to predict the effect of the type and length of SWNTs. In this work, we have thus utilized them to observe the trend and employed the calibrated ONIOM scheme plus the corrected BSSE to examine the chemisorption and apparent activation energies.

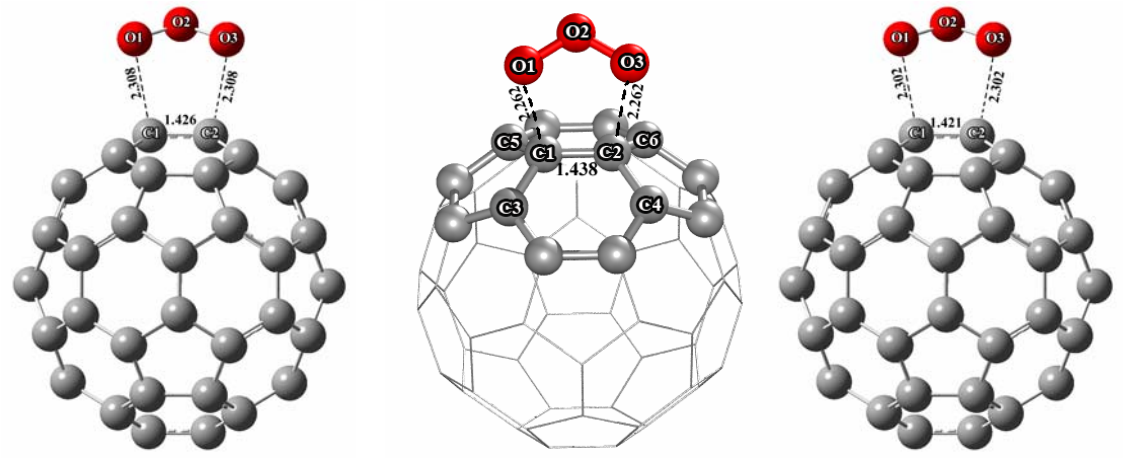

(a) (b) (c)

Figure 22 Optimized geometry of the C_{60}/O_3 at a transition state at the levels of; (a) B3LYP/6-31G (d); (b) ONIOM(B3LYP/6-31G (d):AM1; (c) PBE/def-SV(P).

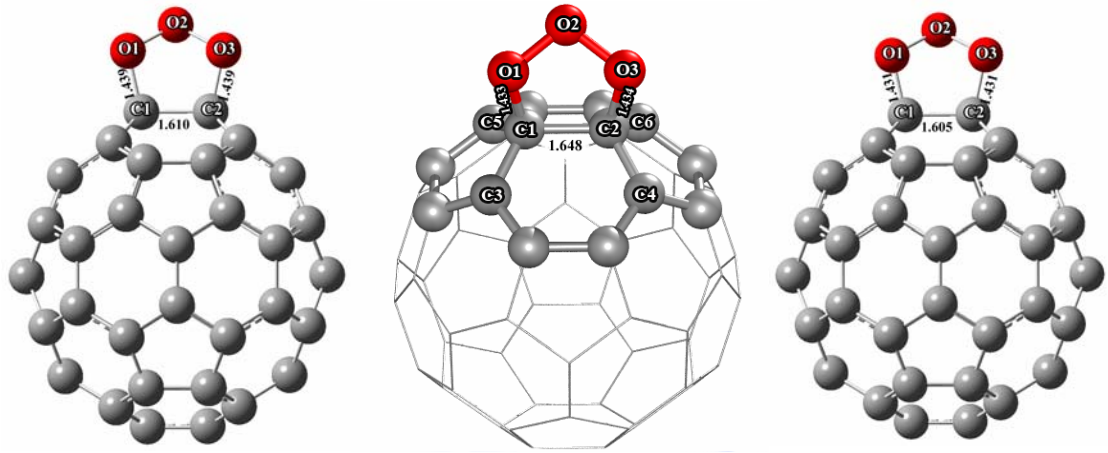

(a) (b) (c)

Figure 23 Optimized geometry of the $C_{60}O_3$ product at the levels of; (a) B3LYP/6-31G (d); (b) ONIOM(B3LYP/6-31G (d):AM1; (c) PBE/def-SV(P).

2.2. The 1,3-dipolar cycloaddition of ozone onto the fullerene hemisphere of capped [5,5]-armchair and [9,0]-zigzag nanotube series

The calculated C1-C2 bond lengths of the transition state structures on the fullerene hemisphere of the capped [5,5]-armchair and [9,0]-zigzag nanotubes are insignificantly different from that of the [60]-fullerene as shown in Figure 23. On the other hand, the bond distances (O1---C1 and O3---C2) that are being formed between ozone and nanotubes are significantly different from the case of [60]-fullerene. The differences found, calculated by using ONIOM/6-31G(d) and PBE/def-SV(P) approaches, are between 0.001 to 0.222 Å for the armchair and 0.002 to 0.166 Å for the zigzag series (cf. Table 3, 4). Therefore the 1,3-dipolar cycloaddition of ozone onto the fullerene hemisphere of the capped nanotubes is considered to follow an asynchronous concerted pathway. As expected from the reactivity indices, the BSSE-corrected activation energies of 1.84-2.78 kcal/mol and 2.16-2.27 kcal/mol for armchair and zigzag nanotubes, respectively (cf. Table 5), are close to that of 2.78 kcal/mol obtained for [60]-fullerene. These values close to the 2.5 kcal/mol of the 1,3-dipolar cycloaddition between 2-*trans*-butene and ozone (Prakash *et al.,* 1980). The exothermic chemisorption energies at the ONIOM(B3LYP/6-31G(d):AM1) are calculated to be 45.92-49.37 kcal/mol and 48.21-48.53 kcal/mol for armchair and zigzag nanotubes, respectively, which are 1-2 kcal/mol more exothermic than that of [60]-fullerene. Also, those at the PBE/def-SV(P) level of theory are 36.59-37.49 kcal/mol and 35.81-38.77 kcal/mol, which are less exothermic than that of ONIOM2 about 10 kcal/mol. The ONIOM2 chemisorption energies are, however, less exothermic by 6-7 kcal/mol as compared to the product reaction energy of ozone and 2-*trans*-butene (Prakash *et al.,* 1980).

In addition to the reactivity at the fullerene hemisphere of the capped nanotubes, an examination of the reactivity at the sidewall of the $C_{90}H_{20}$-armchair nanotube, is made for comparison. It is clearly seen that the reactivity of the 1,3-dipolar cycloaddtion of ozone onto the sidewall of nanotubes (E_a = 6.02 kcal/mol) is significantly lower than that onto the cap-site of nanotubes. This is due to the fact that the curvature, which is measured as a pyramidal angle, at the sidewall (6.0^o) is lower than that at the cap-site (11.6^o).

Increasing the number of the cyclic polyene units shows the same trends as predicted by the reactivity indices. In the armchair series, the ONIOM chemisorption energies slightly fluctuate from -45.92 to -47.65 kcal/mol, for C_{70} to C_{200} whereas they are almost stable at -48.50 kcal/mol for the zigzag series. However, with the capability of the ONIOM method, we might not ensure that this difference, found in the case of [5,5] nanotubes, comes from either the effect of the kind of nanotubes or ONIOM method. For that reason, the PBE approach has be used to monitor it. Subsequently, the PBE chemisorption energies, shown in Table 5 and 6 as well as Figure 25, are almost stable at -37.0 as well for armchair and zigzag series. Besides, the PBE apparent activation energy is approximately steady at -5.0 kcal/mol for both series (cf. Tables 5, 6 and Figure 26).

Furthermore, for the armchair nanotube, the plot of the C1-C2 bond length and the number of cyclic polyene units at the transition state in Figure 24 shows the none oscillation of the C1-C2 bond length at around 1.44 Å for ONIOM(B3LYP/6-31G(d):AM1) and 1.43 Å for PBE/def-SV(P), which is more than those of 1.41 Å and 1.40 Å observed in the nanotube reactant. The constant behavior of the C1-C2 bond length as a function of the number of cyclic polyene is, in addition, found in the zigzag series. So far, we are able to ensure that the type and length of [5,5] armchair and [9,0] zigzag nanotubes do

not have the significant effect to the 1,3-dipolar cycloaddition of ozone and SWNTs capped with [60]-fullerene.

Table 3 Optimized bond lengths (pm) of the 1,3-dipolar cycloadditions of ozone on the geometrical cap of [5,5] single-wall carbon nanotubes capped with fullerene hemisphere at the ONIOM(B3LYP/6-31G(d):AM1) and PBE/def-SV(P) levels of theory.

Species	ONIOM(B3LYP/6-31G(d):AM1)						PBE/def-SV(P)					
	C1-C2		C1-O1		C2-O3		C1-C2		C1-O1		C2-O3	
	TS	Product	TS	Product	TS	Product	TS	Product	TS	Product	TS	Product
C_{60}	143.80	164.81	226.15	143.34	226.25	143.36	142.12	160.51	230.24	143.14	230.24	143.14
C_{70}	144.18	165.02	220.23	143.20	230.13	143.39	143.24	161.02	227.15	143.02	243.65	143.07
C_{80}	142.95	164.98	219.72	143.21	231.85	143.51	143.10	159.87	228.87	142.98	237.86	143.24
C_{90}	143.73	165.32	224.41	143.29	231.77	143.37	142.98	160.34	229.56	143.2	242.12	143.85
C_{100}	144.01	165.30	221.82	143.23	229.94	143.31	143.40	160.77	230.26	142.76	246.12	144.01
C_{110}	143.28	165.17	221.06	143.23	238.61	143.47	143.34	161.01	232.21	142.78	254.12	144.21
C_{120}	143.71	165.27	224.26	143.30	232.21	143.39	142.99	159.68	231.21	143.34	241.01	143.98
C_{130}	143.93	165.33	227.67	143.23	237.03	143.34	143.35	160.31	230.51	142.98	253.21	144.01
C_{140}	143.39	165.05	221.64	143.26	237.51	143.46	143.61	160.34	230.89	143.15	247.35	143.87
C_{150}	143.69	165.19	224.14	143.29	232.67	143.38	143.43	161.07	231.01	142.87	246.34	143.64

Table 3 (Con't)

Species	ONIOM(B3LYP/6-31G(d):AM1)						PBE/def-SV(P)					
	C1-C2		C1-O1		C2-O3		C1-C2		C1-O1		C2-O3	
	TS	Product	TS	Product	TS	Product	TS	Product	TS	Product	TS	Product
C_{160}	143.86	165.30	227.07	143.25	238.31	143.38	143.44	159.86	229.12	143.23	240.13	143.87
C_{170}	143.46	165.29	222.03	143.22	236.64	143.31	143.20	161.11	230.88	143.13	241.75	143.78
C_{180}	143.69	165.17	224.10	143.26	232.87	143.45	143.26	160.45	231.00	142.68	249.14	143.01
C_{190}	143.83	165.27	221.40	143.25	229.43	143.39	143.34	160.34	229.97	142.96	242.31	144.21
C_{200}	143.50	165.20	222.35	143.28	236.13	143.44	143.11	160.64	230.67	143.05	246.32	143.54

Table 4 Optimized bond lengths (pm) of the 1,3-dipolar cycloadditions of ozone on the geometrical cap of [9,0] single-wall carbon nanotubes capped with fullerene hemisphere at the ONIOM(B3LYP/6-31G(d):AM1) and PBE/def-SV(P) levels of theory.

Species	ONIOM(B3LYP/6-31G(d):AM1)						PBE/def-SV(P)					
	C1-C2		C1-O1		C2-O3		C1-C2		C1-O1		C2-O3	
	TS	Product	TS	Product	TS	Product	TS	Product	TS	Product	TS	Product
C_{78}	143.91	165.83	223.03	143.10	231.60	143.33	143.11	160.45	231.01	142.97	245.31	143.25
C_{96}	143.96	166.11	223.46	143.16	230.79	143.15	142.98	161.01	229.36	143.01	246.34	143.78
C_{114}	143.91	166.15	223.60	143.14	233.72	143.24	143.01	159.45	233.31	142.67	250.01	143.01
C_{132}	143.94	166.18	225.87	143.20	232.51	143.20	143.21	160.34	233.12	142.96	246.64	143.75
C_{150}	143.91	166.15	225.29	143.17	232.34	143.23	143.03	160.75	231.69	143.18	248.23	144.01
C_{168}	143.91	166.06	225.66	143.24	232.07	143.24	143.22	161.08	234.15	143.21	244.16	144.11
C_{186}	143.92	166.07	225.04	143.26	231.76	143.22	143.15	160.91	228.97	142.76	239.14	143.45
C_{204}	143.92	166.08	226.35	143.21	231.50	143.25	143.21	160.67	235.64	143.06	247.63	143.95

Table 5 The chemisorption (E_r) and apparent activation (E_a) energies of the 1,3-dipolar cycloadditions of ozone on the geometrical cap of [5,5] single-wall carbon nanotubes capped with fullerene hemisphere.

Species	Chemisorption Energies (E_r)[a] (kcal/mol)		Activation Energies (E_a)[b] (kcal/mol)		
	ONIOM[c]	PBE[e]	ONIOM[c]	BSSE[d]	PBE[e]
C_{60}	-46.26	-37.83	-1.02	2.78	-4.93
C_{70}	-45.92	-37.08	-1.02	2.78	-5.01
C_{80}	-49.37	-36.35	-1.65	1.90	-5.37
C_{90}	-47.62	-37.34	-1.27	2.36	-4.85
C_{100}	-46.94	-36.49	-1.16	1.84	-4.66
C_{110}	-48.78	-36.83	-1.48	2.07	-4.93
C_{120}	-47.64	-37.08	-1.28	2.43	-5.00
C_{130}	-47.11	-37.20	-1.19	2.48	-5.01
C_{140}	-48.46	-37.04	-1.44	2.12	-5.86
C_{150}	-47.68	-37.49	-1.30	2.34	-5.60
C_{160}	-47.26	-36.66	-1.22	2.35	-5.50
C_{170}	-46.95	-37.01	-1.24	2.29	-4.92
C_{180}	-47.70	-37.14	-1.30	2.30	-5.72
C_{190}	-47.36	-36.72	-1.24	2.40	-5.65
C_{200}	-47.65	-36.59	-1.42	2.33	-5.80

[a] E_r = E(adduct) - E(ozone) - E(nanotubes)

[b] E_a = E(transition state complex) - E(ozone) - E(nanotubes)

[c] ONIOM(B3LYP/6-31G(d):AM1)

[d] BSSE at B3LYP6-31G(d)//ONIOM(B3LYP/6-31G(d):AM1)

[e] PBE/def-SV(P)

Table 6 The chemisorption (E_r) and apparent activation (E_a) energies of the 1,3-dipolar cycloadditions of ozone on the geometrical cap of [9,0] single-wall carbon nanotubes capped with fullerene hemisphere.

Species	Chemisorption Energies (E_r)[a] (kcal/mol)		Activation Energies (E_a)[b] (kcal/mol)		
	ONIOM[c]	PBE[e]	ONIOM[c]	BSSE[d]	PBE[e]
C_{78}	-48.28	-38.77	-1.49	2.27	-4.95
C_{96}	-48.21	-37.74	-1.43	2.24	-5.21
C_{114}	-48.51	-35.81	-1.50	2.16	-4.84
C_{132}	-48.42	-37.03	-1.48	2.20	-4.67
C_{150}	-48.53	-37.32	-1.50	2.17	-4.66
C_{168}	-48.44	-36.92	-1.51	2.18	-5.51
C_{186}	-48.49	-37.39	-1.49	2.18	-5.01
C_{204}	-48.49	-36.88	-1.49	2.18	-4.99

[a] E_r = E(adduct) - E(ozone) - E(nanotubes)

[b] E_a = E(transition state complex) - E(ozone) - E(nanotubes)

[c] ONIOM(B3LYP/6-31G(d):AM1)

[d] BSSE at B3LYP6-31G(d)//ONIOM(B3LYP/6-31G(d):AM1)

[e] PBE/def-SV(P)

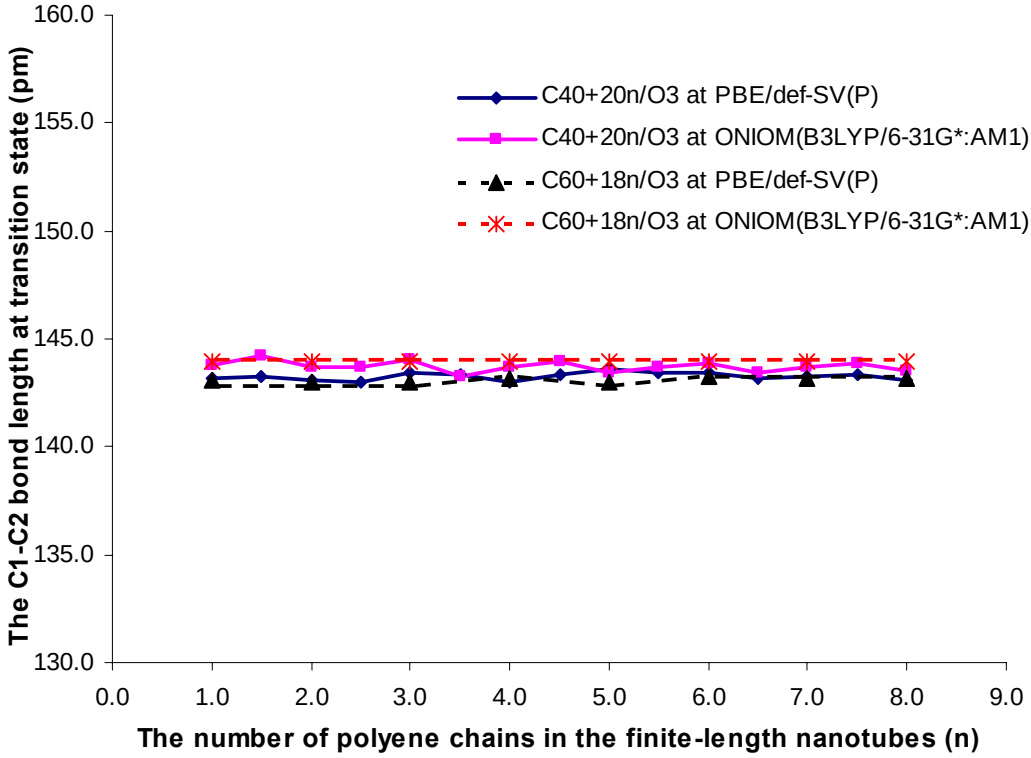

Figure 24 The C1-C2 bond length of nanotubes at transition state structures as a function of n.

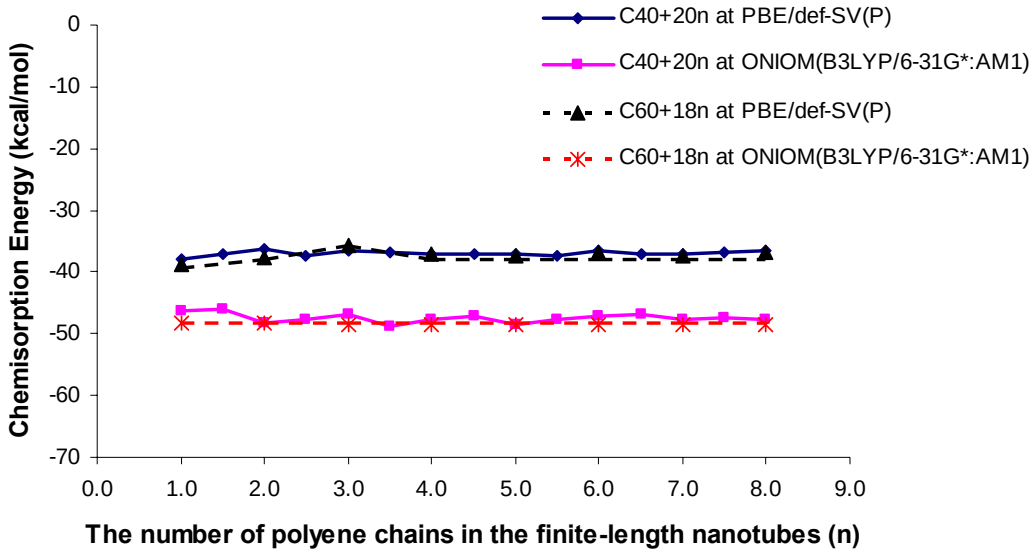

Figure 25 The chemisorption energies of SWNTs-O_3 adducts as a function of n.

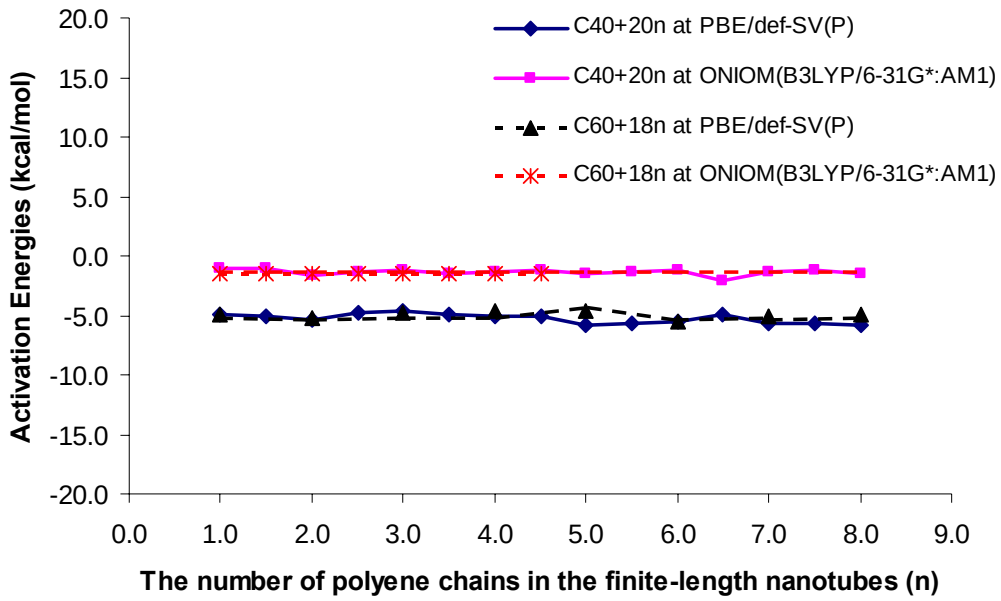

Figure 26 The activation energies of O_3/ SWNT adducts as a function of n.

CONCLUSIONS

The 1,3-dipolar cycloaddition reaction of ozone onto the fullerene hemisphere of [60]-fullerene and two series of the capped [5,5]-armchair and [9,0]-zigzag nanotubes have been investigated by means of the ONIOM(B3LYP/6-31G(d):AM1) and PBE/def-SV(P) schemes. The ONIOM2 absolute chemical hardness of [5,5]-SWNTs is stable at about 0.53 eV, whereas fluctuates and decreases from 0.83 eV to 0.15 eV for the PBE approach when the size of nanotubes is increased from C_{60} to C_{200}. The absolute chemical hardness of [9,0]-SWNTs is steady at 0.53 eV (ONIOM2) and decreases without fluctuation from 0.72 eV to 0.28 eV for C_{78} to C_{204} (PBE). Also, the FMO interaction energy between the LUMO of ozone and HOMO of [5,5]-SWNTs fluctuates from -0.06 to -0.01 eV (ONIOM2) and decreases with the fluctuation behavior from 0.05 eV to -1.05 eV (PBE) for C_{60} to C_{200}. This of [9,0]-SWNTs is, in addition, constant at -0.02 eV (ONIOM) and decreases from -0.22 to -0.94 eV (PBE) for C_{78} to C_{204}, while their activation and chemisorption energies are insensitive to the nanotube length. The activation energies (E_a) of armchair series are between 1.8 to 2.8 kcal/mol, -1.65 to -1.02 kcal/mol, and -5.86 to -4.66 kcal/mol for the BSSE corrected at the B3LYP/6-31G(d), ONIOM(B3LYP/6-31G(d):AM1, and PBE/def-SV(P) methods, respectively. At the same time, in zigzag series, they are between 2.16 to 2.27 kcal/mol, -1.51 to -1.43 kcal/mol, and -5.51 to -4.66 kcal/mol as following such methods. However, the BSSE corrected activation energies are only comparable with experimental estimate of the 2.5 kcal/mol for 2-*trans*-butene. A close inspection of the transition state structures reveals that, for the [60]-fullerene, the reaction mechanism follows the synchronous pathway, whereas, for the armchair and zigzag nanotubes, the reaction proceeds asynchronously. With increasing the number of cyclic polyene units, the exothermic chemisorption energies are of the 45.92-49.37 kcal/mol of ONIOM2 scheme

and the 36.35-37.49 kcal/mol of PBE method in the armchair series. Also, in the case of zigzag series, they are 48.21-48.53 kcal/mol and 35.81-37.74 kcal/mol for ONIOM2 and PBE methods, respectively. Again, the ONIOM2 chemisorption exothermic energies only agree with that of 54.5 kcal/mol reported for 2-*trans*-butene. An additional BSSE corrected ONIOM2 calculation at the sidewall of the armchair nanotube predicts the activation energy for this reaction of 6.03 kcal/mol, which is higher than at the cap end. This leads to a conclusive proof that the most reactive site of the capped carbon nanotubes is located on the fullerene hemisphere. From the PBE and ONIOM results, the type and length of nanotubes do not, in addition, have a significant effect on this reaction.

Finally, our results derived in this study suggest that the PBE method can provide a reliable prediction in electronic reactivity trends, the ONIOM2 sheme is still used to predict the chemisorption energy and the ONIOM2 plus counter point approach is able to provide the activation energy. Furthermore, we believe that with the increasing powerfulness of the computer and theoretical methods, are becoming a more resource-saving and easier accessible route in the exploration of the chemistry of carbon nanotube by providing much instructive information that helps waive a lot of exhausting trial-after-trial experiments in further experimental work.

LITERATURE CITED

Ajayan, P. M. and S. Iijima. 1993. Capillarity-induced filling of carbon nanotubes. **Nature** 361:333-334.

_____, T. W. Ebbesen, T. Ichihashi, S. Iijima, K. Tanigaki and H. Hiura. 1993. Opening carbon nanotubes with oxygen and implications for filling. **Nature** 362:522-525.

_____, 1999. Nanotubes from carbon. **Chem. Rev.** 99:1787-1799.

Bacsa, R., C. Laurent, R. Morishima, H. Suzuki and M. L. Lay. 2004. Hydrogen storage in high surface area carbon nanotubes produced by catalytic chemical vapor deposition. **J. Phys. Chem. B** 108:12718-12723.

Bahr, J. L. and J. M. Tour. 2002. Covalent chemistry of single-wall carbon nanotubes. **J. Mater. Chem.** 12:1952-1958.

Becke, A. D. 1993. Density-functional thermochemistry III: The role of exact exchange. **J. Chem. Phys.** 98:5648-5652.

Bethune, D. S., C. H. Kiang, M. D. de Vries, G. Gorman, R. Savoy, J. Vazquez and R. Beyers. 1993. Cobalt-catalysed growth of carbon nanotubes with single-atomic-layer walls. **Nature** 363:605-607.

Bianco, A., K. Kostarelos, C. D. Partidos and M. Prato. 2005. Biomedical applications of functionalized carbon nanotubes. **Chem. Commun.** 5:571-577.

Boul, P., J. Liu, E. Mickelson, C. Huffman and L. Ericson. 1999. Reversible sidewall functionalization of buckytubes. **Chem. Phys. Lett.** 310:367-372.

Buhl, M., Hirsch, A. 2001. Spherical aromaticity of fullerenes. **Chem. Rev.** 101:1153-1184.

Carroll, D. L., Ph. Redlich, X. Blase, J. C. Charlier, S. Curran, P. M. Ajayan, S. Roth and M. Ruhle. 1998. Effects of nanodomain formation on the electronic structure of doped carbon nanotubes. **Phys. Rev. Lett.** 81: 2332-2335.

Chen, J., M. A. Hammon, H. Hu, Y. S. Chen, A. M. Rao. 1998. Solution properties of single walled carbon nanotubes. **Science** 282:95-98.

Chen, R., Y. Zhang, D. Wang and H. Dai. 2001. Non-covalent sidewall functionalization of single-walled carbon nanotubes for protein immobilization. **J. Am. Chem. Soc.** 23:3838-3839.

Chen, Y., R. C. Haddon, S. Fang, A. M. Rao, P. C. Eklund, W. H. Lee, E. C. Dickey, E. A. Grulke, J. C. Pendergrass, A. Chavan, B. E. Haley and R. E. Smalley. 1998. Chemical attachment of organic functional groups to single-walled carbon nanotube material. **J. Mater. Res.** 13:2423-2431.

Choi, H. J., J. Ihm, S. G. Louie and M. L. Cohen. 2000. Defects, quasibound states, and quantum conductance in metallic carbon nanotubes. **Phys. Rev. Lett.** 84:2917-2920.

Cioslowski, J., N. Rao, D. Moncrieff. 2002. Electronic structures and energetics of [5,5] and [9,0] single-walled carbon nanotubes. **J. Am. Chem. Soc.** 124:8485-8489.

Coleman, S. K., R. S. Bailey, S. Fogden and L. H. M. Green. 2003. Functionalization of single-walled carbon nanotubes via the bingel reaction. **J. Am. Chem. Soc.** 125:8722-8723.

Collins, P. G., A. Zettl, H. Bando, A. Thess, R. E. Smalley. 1997. Nanotube nanodevice. **Science** 278:100-102.

Czerw, R., M. Terrones, J. C. Charlier, X. Blase, B. Foley, R. Kamalakaran, N. Grobert, H. Terrones, P. M. Ajayan, W. Blau, D. Tekleab, M. Ruhle and D. L. Carroll. 2001. Identification of electron donor states in N-doped carbon nanotubes. **Nano Lett.** 1:457-460.

Dai, G., C. Liu, M. Liu, M. Wang and H. Cheng. 2002. Electrochemical hydrogen storage behavior of ropes of aligned single-walled carbon nanotubes. **Nano Lett.** 2:503-506.

Dai, H. 2001. Nanotube growth and characterization carbon nanotubes. **Springer: Berlin** pp 29-53.

Dapprich, S., I. Komaromi, K. S. Byun, K. Morokuma and M. J. Frisch. 1999. A new ONIOM implementation in Gaussian98. Part I. The calculation of energies, gradients, vibrational frequencies and electric field derivatives**. J. Mol Struct. (THEOCHEM)** 461:1-21.

David, W. I. F., R. M. Ibberson, I. C. Matthewman, K. Praaides, T. John, S. Dennis, J. P. Hare, H. W. Kroto, R. Taylor, and D. R. M. Walson. 1991. Crystal structure and bonding of ordered C_{60}. **Nature** 353:147-149.

Dewar, M. J. S., E. G. Zoebisch, E. F. Healy and J. J. P. Stewart, 1984. Development and use of quantum mechanical molecular models AM1: a new general purpose quantum mechanical molecular model. **J. Am. Chem. Soc.** 107:3902-3909.

Ebbesen, T. W. and P. M. Ajayan. 1992. Large-scale synthesis of carbon nanotubes. **Nature** 358:220–222.

Eichkorn, K., O.Treutler, H.Oehm, M.Haeser and R.Ahlrichs. 1995. **Chem. Phys. Lett.** 242:652-660.

Elango, M, R Parthasarathil, G. K. Narayanan, A M. Sabeelullah, U. Sarkar, N. S. Venkatasubramaniyan, V. Subramanian and P. K. Chattaraj. 2005. Relationship between electrophilicity index, Hammett constant and nucleus-independent chemical shift. **J. Chem. Sci.** 117:61–65.

Frisch, M.J., G. W. Trucks, H. B. Schlegel, G. E. Scuseria, M. A. Robb, J. R. Cheeseman, J. A. Montgomery, Jr., T. Vreven, K. N. Kudin, J. C. Burant, J. M. Millam, S. S. Iyengar, J. Tomasi, V. Barone, B. Mennucci, M. Cossi, G. Scalmani, N. Rega, G. A. Petersson, H. Nakatsuji, M. Hada, M. Ehara, K. Toyota, R. Fukuda, J. Hasegawa, M. Ishida, T. Nakajima, Y. Honda, O. Kitao, H. Nakai, M. Klene, X. Li, J. E. Knox, H. P. Hratchian, J. B. Cross, V. Bakken, C. Adamo, J. Jaramillo, R. Gomperts, R. E. Stratmann, O. Yazyev, A. J. Austin, R. Cammi, C. Pomelli, J. W. Ochterski, P. Y. Ayala, K. Morokuma, G. A. Voth, P.

Salvador, J. J. Dannenberg, V. G. Zakrzewski, S. Dapprich, A. D. Daniels, M. C. Strain, O. Farkas, D. K. Malick, A. D. Rabuck, K. Raghavachari, J. B. Foresman, J. V. Ortiz, Q. Cui, A. G. Baboul, S. Clifford, J. Cioslowski, B. B. Stefanov, G. Liu, A. Liashenko, P. Piskorz, I. Komaromi, R. L. Martin, D. J. Fox, T. Keith, M. A. Al-Laham, C. Y. Peng, A. Nanayakkara, M. Challacombe, P. M. W. Gill, B. Johnson, W. Chen, M. W. Wong, C. Gonzalez, and J. A. Pople. 2003. **Gaussian 03.** Gaussian, Inc, Pittsburgh, PA.

Georgakilas, V., K. Kordatos, M. Prato, D. M. Guldi, M. Holzinger and A. Hirsch. 2002. Organic functionalization of carbon nanotubes. **J. Am. Chem. Soc.** 124:760-761.

_____, N. Tagmatarchis, D. Pantarotto, A. Bianco, J. Briand and M. Prato. 2002. Amino acid functionalization of water soluble carbon nanotubes. **Chem. Commun.** 24:3050-3051.

Gillies, J. Z., C. W. Gillies, R. D. Suenram and F. J. Loves. 1988. The ozonolysis of ethylene. Microwave spectrum, molecular structure, and dipole moment of ethylene primary ozonide (1,2,3-trioxolane). **J. Am. Chem. Soc.** 110:7991-7999.

Haddon, R. C. 1993. Chemistry of the Fullerenes: The Manifestation of Strain in a Class of Continuous Aromatic Molecules. **Science** 261:1545-1550.

_____, G. E. Scuseria and R. E. Smalley. 1997. C240-The most chemically inert fullerene? **Chem. Phys. Lett.** 272:38-42.

Hamada, N., S. Sawada and A. Oshiyama. 1992. New one-dimensional conductors: graphite microtubules. **Phys. Rev. Lett.** 68:1579-1581.

Hamon, M. A., M. E. Itkis, S. Niyogi, T. Alvaraez, C. Kuper, M. Menon and R. C. Haddon. 2001. Effect of rehybridization on the electronic structure of single-walled carbon nanotubes. **J. Am. Chem. Soc.** 123:11292-11293.

Hendrickx, F. A. M. and C. Vinckier. 2003. 1,3-Cycloaddition of ozone to ethylene, benzene, and phenol: A comparative ab initio study. **J. Phys. Chem. A** 107:7574-7580.

Heymann, D., S. M. Bachilo, R.B. Weisman, F. Cataldo, R.H. Fokkens, N. M. M. Nibbering, R. D. Vis and L. P. F. Chibante. 2000. $C_{60}O_3$, a fullerene ozonide: synthesis and dissociation to $C_{60}O$ and O_2**. J. Am. Chem. Soc.** 122:11473-11479.

Hirsch, A. 2002. Functionalization of single-walled carbon nanotubes. **Angew. Chem., Int. Ed.** 41:1853-1859.

Holzinger, M. O. Vostrowsky, A. Hirsch, F. Hennrich, M. Kappes, R. Weiss and F. Jellen. 2001. Sidewall functionalization of carbon nanotubes. **Angew. Chem., Int. Ed.** 40:4002-4005.

_____, J. Abraham, P. Whelan, R. Graupner, L. Lothar, F. Hennrich, M. Kappes and A. Hirsch. 2003**.** Functionalization of single-walled carbon nanotubes with (R-)oxycarbonyl nitrenes. **J. Am. Chem. Soc**. 125:8566-8580.

Hu, H., B. Zhao, A. M. Hamon, K. Kamaras, E. M. Itkis and C. R. Haddon. 2003. Sidewall functionalization of single-walled carbon nanotubes by addition of dichlorocarbene. **J. Am. Chem. Soc.** 125:14893-14900.

Iijima, S. 1991. Helical microtubules of graphitic carbon. **Nature** 354:56-58.

_____, P.M. Ajayan and T. Ichiashi, 1992. Growth model for carbon nanotubes. **Phys. Rev. Lett.** 69:3100-3103.

_____, and T. Ichihashi. 1993. Single-shell carbon nanotubes of 1-nm diameter. **Nature** 363:603-605.

Journet, C., W. K. Maser, P. Bernier, A. Loiseau, M. Chapelle, S. Lefrant, P. Deniard, R. Lee and J. E. Fischer. 1997. Large-scale production of single-walled carbon nanotubes by the electric-arc technique. **Nature** 388:756 – 758.

Kazaoui, S., N. Minami, R. Jacquemin, H. Kataura and Y. Achiba. 1999. Amphoteric doping of single-wall carbon-nanotube thin films as probed by optical absorption spectroscopy**. Phys. Rev. B** 60:13339-13342.

_____, N. Minami, N. Matsuda, H. Kataura and Y. Achiba. 2001. Electrochemical tuning of electronic states in single-wall carbon nanotubes studied by in situ absorption spectroscopy and ac resistance. **App. Phys. Lett.** 78: 3433-3435.

Khabashesku, V. N.,W. E. Billups and J. L. Margrave. 2002. Fluorination of single-wall carbon nanotubes and subsequent derivatization reactions. **Acc. Chem. Res.** 35:1087-1095.

Kam, W. S. N., C. T. Jessop, A. P. Wender and H. Dai. 2004. Nanotube molecular transporters: internalization of carbon nanotube-protein conjugates into mammalian cells. **J. Am. Chem. Soc.** 126:6850-6851.

Kong, J., H. Soh, A. Cassell, C. F. Quate and H. Dai.1998. Synthesis of individual single-walled carbon nanotubes on patterned silicon wafers. **Nature** 395:878-881.

Koshio, A., M. Yudasaka and S. Iijima. 2002. Thermo gravimetric analysis of single-wall carbon nanotubes ultrasonicated in monochlorobenzene. **Chem. Phys. Lett.** 364:420-426.

Kroto, H. W. J. R. Heath, S. C. O'Brien, R. F. Curl and R. E. Smalley. 1985. C_{60}: Buckminsterfullerene. **Nature** 318:162-163.

Lan, A. and A. Mukasyan. 2005. Hydrogen storage capacity characterization of carbon nanotubes by a micro gravimetrical approach. **J. Phys. Chem. B** 109:16011-16016.

Lee, C., W. Yang, and R. G. Parr. 1988. Development of the Colle-Salvetti correlation-energy formula into a functional of the electron density**.** **Phys. Rev. B** 37: 785-789.

Lee, S. M., K. H. An,Y. H. Lee, G. Seifert and T. Frauenheim. 2001. A hydrogen storage mechanism in single-walled carbon nanotubes. **J. Am. Chem. Soc.** 123:5059-5063.

Lu, X., F. Tian, N. Wang and Q. Zhang. 2002. Organic functionalization of the sidewalls of carbon nanotubes by diels-alder reactions: a theoretical prediction. **Org. Lett.** 24:4313-4315.

_____, F. Tian, X. Xu, N. Wang and Q. Zhang. 2002. Sidewall oxidation and complexation of carbon nanotubes by base-catalyzed cycloaddition of transition metal oxide: a theoretical prediction**. Nano Lett.** 2:1325-1327.

_____, L. Zhang, X. Xu, N. Wang and Q. Zhang 2003. Can the sidewalls of single-wall carbon nanotubes be ozonized? **J. Phys. Chem. B** 106:2136-2139.

_____, F. Tian, X. Xu, N. Wang and Q. Zhang. 2003. A theoretical exploration of the 1,3-dipolar cycloadditions onto the sidewalls of [n,n] armchair single-walled carbon nanotubes. **J. Am. Chem. Soc.** 125:10459-10464.

Martin, N., M. Altable, S. Filippone, A. M. Domenech, L. Echegoyen and C. M. Cardona. 2006. Retro-cycloaddition reaction of pyrrolidinofullerenes. **Angew. Chem. Int. Ed.** 45:110-114.

Matsuo, Y., K. Tahara and E. Nakamura. 2003. Theoretical studies on structures and aromaticity of finite-length armchair carbon nanotubes. **Org. Lett.** 5:3181-3184.

Mawhinney, D. B., V. Naumenko, A. Kuznetsova, J. T. Yates, J. Liu and R. E. Smalley. 2000. Infrared spectral evidence for the etching of carbon nanotubes: ozone oxidation at 298 k. **J. Am. Chem. Soc.** 122:2383-2384.

McKee, M. L. and C. M. Rohlfing. 1981. An ab initio study of complexes between ethylene and ozone. **J. Am. Chem. Soc.** 111:2497-2500.

Mickelson, E. T., C. B. Huffman, A. G. Rinzler, R. E. Smalley, R. H. Hauge and J. L. Margrave.1998. Fluorination of single-wall carbon nanotubes. **Chem. Phys. Lett.** 296:188-194.

Mintmire, J. W., B. I. Dunlap and C. T. White. 1992. Are fullerene tubules metallic? **Phys. Rev. Lett.** 68:631-634.

Namuangruk, S., P. Pantu and J. Limtrakul. 2004. Alkylation of benzene with ethylene over faujasite zeolite investigated by the ONIOM method. **J. Cat**. 225:523-530.

_____, P. Pantu and J. Limtrakul. 2005. Investigation of ethylenedimerization over faujasite zeolite by the ONIOM method**. ChemPhysChem** 6:1333-1339.

Neeb, P., O. Horie and K.G. Moortgat.1998. The ethene-ozone reaction in the gas phase. **J. Phys. Chem. A** 102:6778-6785.

Niyoki, S., M. A. Hamon, H. Hu, B. Zhao, P. Bhowmik, R. Sen, M. E. Itkis, R.C. Haddon. 2002. Chemistry of single-walled carbon nanotubes. **Acc. Chem. Res.** 35:1105-1113.

O'Connell, M. J., P. Boul, L. M. Ericson, C. Huffman and Y. Wang. 2001. Reversible water-solubilization of single-walled carbon nanotubes by polymer wrapping. **Chem. Phys. Lett.** 342:265-271.

Odom, T. W., J. L. Huang, P. Kim, M. Ouyang and C. M. Lieber. 1998. Scanning tunneling microscopy and spectroscopy studies of single-walled carbon nanotubes. **J. Mater. Res.** 13:2380-2388.

_____, J. L. Huang, P. Kim and C. M. Lieber. 1998. Atomic structure and electronic properties of single-walled carbon nanotubes. **Nature** 391:62-64.

Ouyang, M., L. J. M. Huang and M. C. Lieber. 2002. Fundamental electronic properties and applications of single-walled carbon nanotubes. **Acc. Chem. Res.** 35:1018-1025.

Prakash, S. N. and W.B. Sidney. 1980. Thermochemistry and kinetics of ozonation reactions. **J. Am. Chem. Soc.** 102:3105-3115.

Peng, H., B. Alemany, L. J. Margrave and N. V. Khabashesku. 2003. Nanotube molecular transporters: internalization of carbon nanotube-protein conjugates into mammalian cells. **J. Am. Chem. Soc.** 125:15174-15182.

_____, P. Reverdy, V. N. Khabashesku and J. L. Margrave. 2003. Sidewall functionalization of single-walled carbon nanotubes with organic peroxides. **Chem. Commun.** 3:362-363.

Perdew, J. P. and Y. Wang. 1992. Accurate and simple analytic representation of the electron-gas correlation energy. **Phys. Rev. B** 45:13 244-13249.

_____, J. P., K. Burke, and M. Ernzerhof. 1996. Generalized Gradient Approximation Made Simple. **Phys. Rev. Lett.** 77:3865-3868.

Petit, P., C. Mathis, C. Journet, P. Bernier. 1999. Tuning and monitoring the electronic structure of carbon nanotubes. **Chem. Phys. Lett.** 305:370-374.

Ruther, M. G., F. Frehill, J. E. O'Brien, A. I. Minett, W. J. Blau and J. G. Vos. 2004. Characterization of covalent functionalized carbon nanotubes. **J. Phys. Chem. B** 108:9665-9668.

Saini, R. K., I. W. Chiang, H. Peng, R. E. Smalley, W. E. Billups, R. H. Hauge and J. L. Margrave. 2003. Covalent sidewall functionalization of single-walled carbon nanotubes. **J. Am. Chem. Soc.** 125:3617-3621.

Saito, R., R. Saito, M. Fujita, G. Dresselhaus and M. S. Dresselhaus. 1992. Electronic-structure of chiral graphene tubules. **Appl. Phys. Lett.** 60:2204-2206.

Sander J. T., R. M. Alwin and C. Dekker. 1998. Room-temperature transistor based on a single carbon nanotubes. **Nature** 393:49–52.

Schleyer, P. V. R., C. Maerker, A. Dransfeld, H. Jiao and N. E. Hommes. 1996. Nucleus-Independent Chemical Shifts: A Simple and Efficient Aromaticity Probe. **J. Am. Chem. Soc.** 118:6317-6318.

Sondheimer, F., Y. Gaoni, L. M. Jackman, N. A. Bailey and R. Mason. 1996. 1,8-Bisdehydro [4] Annulene, an Unusual Aromatic Compound. **J. Am. Chem. Soc.** 84:4595-4596.

Stanislaus S. W., E. Joselevich, A. T. Woolley, C. L. Cheung and C. M. Lieber. 1998. Covalently functionalized nanotubes as nanometre-sized probes in chemistry and biology. **Nature** 394:52–55.

Star, A., J. Stoddart, D. Steuerman, M. Diehl and A. Boukai. 2001. Preparation and properties of polymer-wrapped single-walled carbon nanotubes. **Angew. Chem., Int. Ed.** 40:1721-1725.

Sun, Y., K. Fu, Y. Lin and W. Huang. 2002. Functionalized carbon nanotubes:properties and applications. **Acc. Chem. Res.** 35:1096-1104.

Taylor, R. and D. M. R Walton. 1993. The Chemistry of the Fullerenes. **Nature** 363:685-687.

Tang, S. C., Harris, P. J. F. and Green, M. L. H. 1993. Thinning and opening of carbon nanotubes by oxidation using carbon dioxide. **Nature** 362:520-522.

Venerma, L.C., Meunier, V. Lambin, P. Dekker and C. Datum. 2000. Atomic structure of carbon nanotubes from scanning tunneling microscopy. **Phys. Rev. B** 61:2991-2996.

Warakulwit, C., S. Bamrungsap, P. Luksirikul, P. Khongpracha and J. Limtrakul. 2005. Diels-Alder cycloadditions of single-wall carbon nanotubes with electron-rich dienes: a theoretical study. **Stud. Surf. Sci. Catal.** 156:823-828.

Wildoer, J. W. G., L. C. Venema, A. G. Rinzler, R. E. Smalley and C. Dekker. 1998. Electronic structure of atomically resolved carbon nanotubes. **Nature** 391:59-62.

Yamashita, J., H. Hirayama, Y. Ohshima and K. Takayanagi. 1999. Growth of a single-wall carbon nanotube in the gap of scanning tunneling microscope. **Appl. Phys. Lett.** 74:2450-2452.

Ying, Y., R. K. Saini, F. Liang, A. K. Sadana and W. E. Billups. 2003. Functionalization of carbon nanotubes by free radicals. **Org. Lett.** 5:1471-1473.

Yumura, T., K. Hirahara, S. Bandow, K. Yoshizawa and S. Iijima. 2004. A theoretical study on the geometrical features of finite-length carbon nanotubes capped with fullerene hemisphere. **Chem. Phys. Lett.** 386:38–43.

Zhang, X., D. Cao and J. Chen. 2003. Hydrogen adsorption storage on single-walled carbon nanotube arrays by a combination of classical potential and density functional theory. **J. Phys. Chem. B** 107:4942-4950.

Zhou, O., S., Hideo, G. Bo, S. OH, L. Fleming and G. Yue. 2002. Materials science of carbon nanotubes: fabrication, integration, and properties of macroscopic structures of carbon nanotubes. **Acc. Chem. Res**. 35:1045-1053.

Zhu, J., J. Kim, H. Peng, J. L. Margrave, V. N. Khabashesku and E. V. Barrera. 2003. Improving the dispersion and integration of single-walled carbon nanotubes in epoxy composites through functionalization. **Nano Lett.** 3:1107-1113.

CURRICULUM VITAE

NAME : Mr. Montree Sawangphruk

BIRTH DATE : August 3, 1980

BIRTH PLACE : Roi Et, Thailand

EDUCATION :

YEAR	**INSTITUTION**	**DEGREE/DIPLOMA**
2003	Ubonrathchathani Univ.	B.S. (Chemistry) with second class honors

SCHOLASHIP : Chumbhot-Pantip Foundation (1998-2002)

The Ministry of University Affairs under the Science and Technology Higher Education Development Project (2002-2004)

The higher educational strategic scholarships for frontier research network (2005-2010)